STUDIES ON MATHEMATICAL MODELING OF MIDDLE EAR GAS EXCHANGE

by

Stephen Chad Kanick

BS in Chemical Engineering, West Virginia University, 2002

Submitted to the Graduate Faculty of

the School of Engineering in partial fulfillment

of the requirements for the degree of

Master of Science in Chemical Engineering

University of Pittsburgh

2004

UNIVERSITY OF PITTSBURGH

SCHOOL OF ENGINEERING

This thesis was presented

by

Stephen Chad Kanick

It was defended on

August 18, 2004

and approved by

Sachin Velankar, Assistant Professor, Department of Chemical and Petroleum Engineering

Thesis Co-advisor: Joseph J. McCarthy, Associate Professor, Department of Chemical and Petroleum Engineering

Thesis Co-advisor: William J. Doyle, Professor, Department of Otolaryngology, School of Medicine

STUDIES ON MATHEMATICAL MODELING OF MIDDLE EAR GAS EXCHANGE

Stephen Chad Kanick, MS

University of Pittsburgh, 2004

Middle ear (ME) pressure regulation is a topic of fundamental interest to the pediatric otolaryngology community since a lack of proper regulation is a precursor to middle ear disease. Development of mathematical models of ME gas exchange can improve understanding of the underlying ME physiology. Previous models were limited in their description of gas exchange (based on inputted empirical exchange constants) and in their application (few models posses capacity for clinical relevance in diagnosis). Here, we present investigations which improve and expand on previous models.

The first study presents a global description of ME pressure regulation and applies the model to flight-related barotrauma. While a well functioning Eustachian tube has long been known to protect from barotrauma, the simulation results show that a variety of buffering mechanisms can reduce the demand placed on the efficiency of that function. Using these results, subclasses of ears with little risk for barotrauma were identified and an algorithm was developed that makes these assignments based on measurable variables.

The second study outlines and analyzes a morphometric approach to describing transmucosal gas exchange within the middle ear. Implementation of the morphometric model requires the measurement of diffusional length (τ) for the ME mucosa which contributes to the mucosal diffusing capacity, a measure of the resistance to gas flow between airspace and capillary. Two methods for measuring τ have been proposed: the linear distance between air-mucosal boundary

and capillary as described by Ars and colleagues, and the harmonic mean of all contributing pathway lengths as described by Weibel and colleagues. Here, oxygen diffusing capacity was calculated for different ME mucosal geometries using the two τ measures, and the results were compared to those predicted by a 2-dimensional finite element analysis. Predictive accuracy was improved by incorporating the τ measure described by Weibel which captures important information regarding variations in capillary shape and distribution. However, when compared to the oxygen diffusing capacity derived from the finite element analysis, both measures yielded non-linear, positively biased estimates. The morphometric techniques underestimate diffusion length by failing to account for the curvilinear gas flow pathways predicted by the finite element model.

TABLE OF CONTENTS

LIST OF TABLES

LIST OF FIGURES

PREFACE

I have enjoyed my time working at the ENT department of Pittsburgh's Children's Hospital. First off, and most importantly, I would like to thank my family for their support throughout my twenty-four years. During my studies in Pittsburgh, I am grateful to the following: to William Doyle for his mentorship, patience and generous amounts of time (including weekly meetings at Peter's Pub and the excursion to Sandbridge) where he shared insights on philosophy, medicine and grammar, to Douglas Swarts for the many hours of conversations (with topics ranging from science to soccer) and his constant support throughout, to Joseph McCarthy for providing insight and advice far before he ever received the title 'advisor', to Samir Ghadiali for offering help when I was a novice first-year, and to my Children's hospital co-workers (Julie Banks, Jim Seroky, Sancak Yuksel, Cathy Lo, and Darleen Noah) who made my experience not only successful but also enjoyable.

The funding for my time here was paid for in part by a Grant the NIH (NIDCD 01250) and by support from the 2003 NASA Space Grant Fellowship.

1.0 INTRODUCTION

Development of mathematical models of ME (middle ear) gas exchange can improve understanding of the underlying ME physiology. Here, we begin with a mathematical model of middle ear pressure regulation based on known physiological mechanisms and apply the model to flight-related barotrauma. Our goals of this investigation are to clarify the mechanism underlying the pathogenesis of barotrauma during pressurized air-flight and to develop heuristic rules that assign risk for individual ears.

Later, we perform a critical analysis of the transmucosal component of middle ear gas exchange. Within the global ME system model, transmucosal exchange is governed by inputted species-specific empirical time constants and therefore is not applicable to all physiologic states. This shortcoming could be eliminated through application of a morphometric model which incorporates more fundamental physiochemical and anatomical parameters from which the species time-constants can be derived for all extant conditions. We go on to investigate the development of the morphometric model within the ME mucosal system, and then analyze the effect which morphometric measurement techniques for diffusion length have on predictions of mucosal diffusing capacity.

1.1 BAROTRAUMA DEVELOPMENT DURING AIRPLANE FLIGHT

Barotrauma, the most common medical disorder associated with modern air travel, affects an estimated 5 percent of adult and 25 percent of child passengers [1]. Two primary expressions of barotrauma can be distinguished based on signs and pathophysiology; barotitis media and

baromyringitis. Barotitis media is middle ear mucosal (MEM) inflammation, hemorrhage and leakage of transudate into the middle ear airspace (ME) precipitated by moderate ME underpressures relative to the surrounding MEM. Baromyringitis is damage to the tympanic membrane (TM) with severe pain caused by large pressure differences between ME and cabin. Sequelae of barotrauma can include deafness, dizziness and tinnitus [2, 3].

Many previous studies describing the pathogenesis of barotrauma were done on divers or on patients being treated in hyperbaric O_2 chambers [4-7] , situations that do not share the physiological conditions experienced during pressurized flight. Moreover, most publications and reviews that specifically focused on barotrauma during flight lack empirical data and described disease pathogenesis using broad generalizations [3, 8-10]. For this reason, counter-intuitive observations (e.g. apparent protective effect of pre-existing disease) were interpreted in the absence of physiological representation, a situation that complicates clinical decision-making with respect to risk assessments [11, 12]. Here, we approach the subject from the perspective of basic physiology using both descriptive and mathematical formats. Our goals are to clarify the mechanism underlying the pathogenesis of barotrauma during pressurized flight and to develop heuristic rules that assign risk for individual ears.

1.1.1 Middle Ear Pressure Regulation

Barotrauma is caused by an inability to maintain near pressure equivalence between the ME and airplane cabin as the latter is changed rapidly during ascent and descent. Normally, the pressure of the fluid-free ME is near ambient ($P_{ME} \approx P_{AMB} \approx P_{Cabin}$) which ensures free vibration of the TM and efficient transduction of sound energy to the inner ear. Because the ME is usually a closed, relatively non-collapsible, temperature stable, mucosal-lined bony cavity, its pressure is a

direct function of the contained gas volume, and gas transfer to or from the ME affects its pressure.

Table 1-I List of Abbreviations.

Abbreviation	*Term*
ME	Middle ear airspace
MEM	Middle ear mucosa
ET	Eustachian tube
TM	Tympanic membrane
NP	Nasopharynx
IE	Inner ear
mTVP	Tensor veli palatine muscle
VAS	Vascular
AMB	Ambient
typ	Tympanum
mas	Mastoid

The ME consists of two functionally discrete but continuous airspaces: the anterior, tympanum which contains the ossicles, ligaments and muscles of the sound transducer mechanism, and the posterior, mastoid cavity which is subdivided into numerous intercommunicating air-cells [13]. While the variance among individuals and age groups in tympanum volume is low ($V_{tym} \approx 1$ ml.), that of the mastoid is large ($V_{mas} \approx 0 - 15$ ml) due to contributions of age, gender and disease history effects [14, 15]. The anterior wall of the tympanum is continuous with the osseous portion of the Eustachian tube (ET), the lateral wall includes the TM, the medial wall includes the round window membrane, and the posterior wall opens to the mastoid airspace by way of a large air-cell, the antrum [13].

Figure 1.1 shows the various gas exchange pathways for the ME when isolated within an airplane cabin. The tympanum can exchange gas with the external environment via the TM and with the inner ear via the round window, but experimental measurements show that gas exchange

across these pathways is negligible [16, 17]. Therefore, in describing ME pressure-regulation, the physiologically relevant pathways are: tympanum-antrum-mastoid, ME-MEM-blood and tympanum-ET-nasopharynx (NP). Because the tympanum and mastoid are continuous in the airphase, total pressure differentials are rapidly equilibrated and established gas partial-pressure differentials decay quickly [18]. In contrast, ME-MEM-blood gas exchange is a diffusive process whose rate depends on the extant partial-pressure gradients and gas specific exchange constants [19-21].

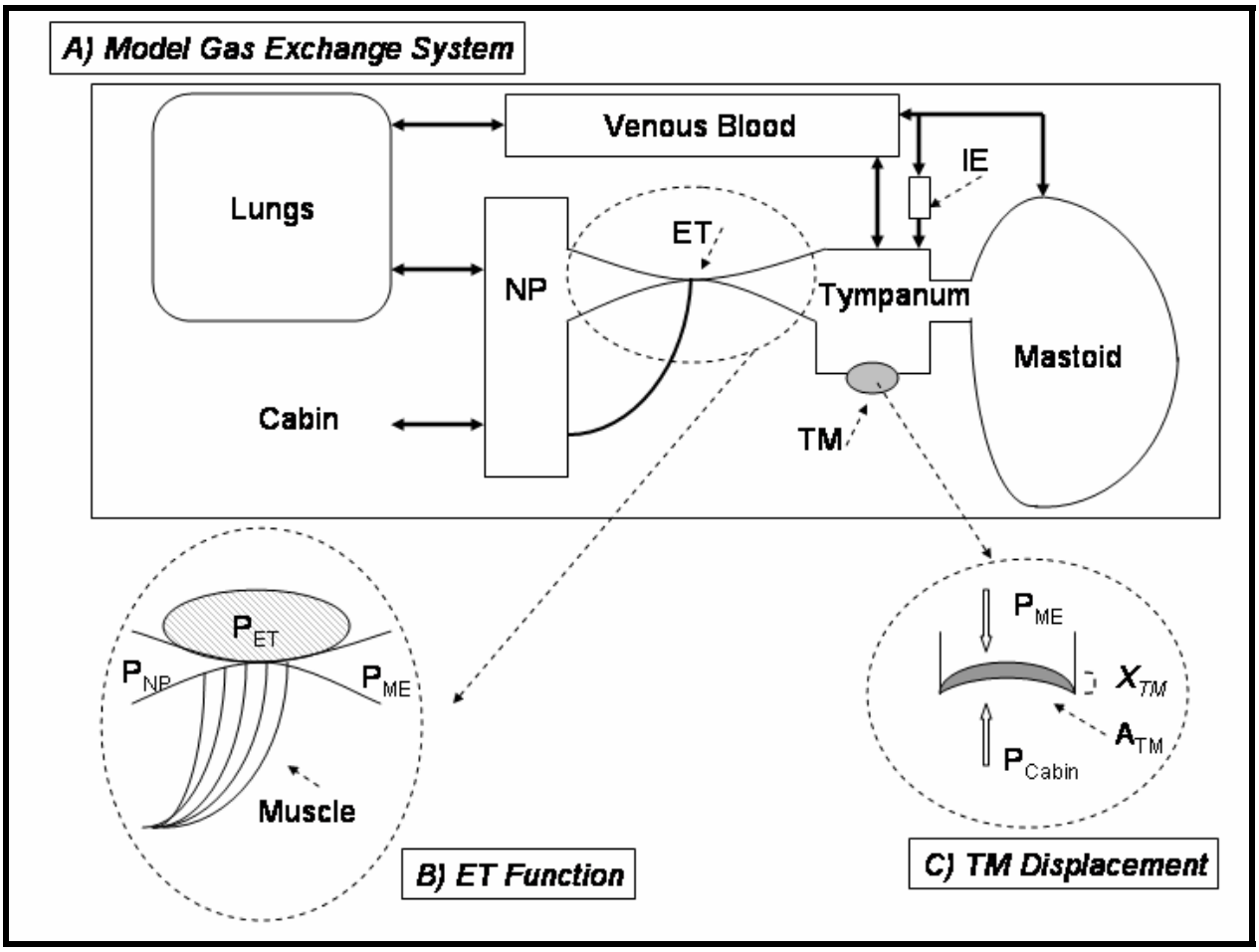

Figure 1.1: A cartoon illustrating the pathways for ME gas exchange (a), the factors contributing to passive (via pressure induced flow past a compressing balloon) and active (via mTVP muscle contraction) ET function (b), and the effect of ME-ambient pressure gradients on TM displacement (c). See text for details.

At physiological partial-pressure gradients between ME and venous blood (VB), gas exchange across this path is primarily attributable to the relatively slow exchange of N_2 and, consequently this exchange is expected to have a minimal effect on ME pressure over most flight durations.

However, gas exchange across the ET is a rapid, gradient dependent, bolus exchange of mixed gases between NP and tympanum. Under normal physiological conditions, this is the only potential direct communication between ME and ambient environment and the only exchange pathway capable of reducing established positive, ambient-ME pressure gradients.

The functional anatomy of the ET has been described in many publications [9, 13, 22, 23]. Briefly, the posterior portion of the ET is a mucosa lined, bony tube continuous with the anterior tympanum while the anterior portion is cartilaginous medially and membranous laterally (Figure 1.2). The cartilaginous portion is usually closed by a tissue pressure, P_{ET} that equals the sum of the ambient pressure (P_{AMB} - a consequence of the incompressibility of body fluids) and a vascular pressure (P_{VAS}) [23, 24]. A muscle, the tensor veli palatini (mTVP) takes origin from the membranous wall of the ET and terminates on the hamular process and within the palatine aponeurosis [13]. Activation of the muscle during swallowing exerts an anterior-lateral-inferior vector force (F_{TVP}) on the membranous wall of the ET [22].

Figure 1.1b depicts these functional relationships. There, the ET is represented as a balloon pressure valve that is normally closed by the pressure difference between P_{ET} and both P_{NP} and P_{ME}. ET opening can be effected by passive, pressure-driven processes or by active, pressure-driven or muscle-assisted mechanisms [25, 26]. Passive, pressure-driven ET opening occurs when either P_{ME} or P_{NP} exceeds P_{ET} which forces the ET lumen open (displaces the balloon walls shown in Figure 1.1b). Active, pressure-driven ET opening occurs when P_{NP} is

increased to greatly exceed the P_{ET} during Valsalva and Toynbee maneuvers, or for some individuals, when P_{ET} is reduced by yawning or mandibular repositioning [13, 23, 26, 27].

Active, muscle-assisted ET opening occurs when the mTVP contracts with sufficient force (F_{TVP}) to overcome the force exerted by P_{ET} and other forces attributable to intraluminal surface tension (F_{ST}) [13, 24, 28]. The teleological effect of these "normal" ET openings is to allow NP-ME gas exchange so as to maintain a quasi-steady state pressure equivalence between P_{ME} and P_{AMB} as P_{ME} is decreased by transmucosal gas exchange and P_{AMB} fluctuates with barometric conditions; i.e. normal ME pressure-regulation [13, 29, 30].

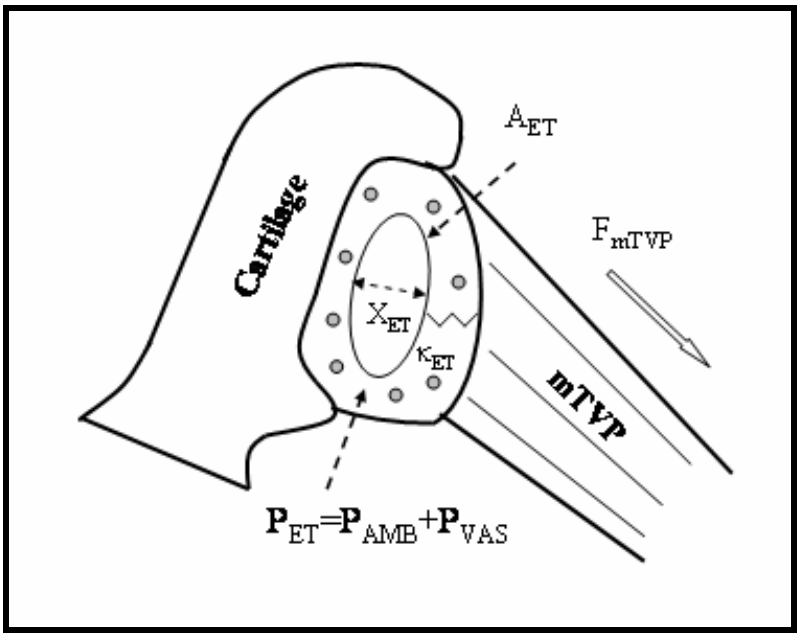

Figure 1.2: Component forces acting on the ET during active, muscle-assisted openings. The lumen remains open until the force of the surrounding tissue (a function of tissue pressure, P_{ET} and contact area, A_{ET}) exceeds that exerted by the mTVP. Airflow through the ET is a function of the cross-sectional area of the lumen, related to the width opened, shown as X_{ET}, and is determined in part by the of mechanical stiffness of the lumen and surrounding tissue, shown as K_{ET}.

Movements of the TM in response to ME-ambient pressure differentials are an important exception to the assumed fixed ME volume. There, small fluctuations in that gradient can be

absorbed by ME volume changes in response to pressure-driven TM movements [15, 31]. This is illustrated in Figure 1.1c which shows the TM response to a ME-Cabin pressure gradient. As given by Boyles law (where PV = constant for a closed system), the magnitude of this pressure buffering effect is a function of the ratio of TM volume displacement to ME volume. In healthy ears, the maximum TM displacement volume is approximately 1% of the ME (i.e. tympanum + mastoid) volume [15] and the buffering effect of TM displacement on ME pressure is limited. However, persistent ME disease causes a significantly reduced mastoid volume and can cause a hyper-compliant TM [32, 33], changes that will increase the determinate ratio for TM buffering and may reduce the affected MEs susceptibility to barotrauma.

1.1.2 Normal ME Pressure Regulation during Flight

During airplane ascent, P_{Cabin} decreases which causes decreasing P_{NP}, P_{ET} and P_{MEM} while P_{ME} is relatively unchanged *vis a vis* takeoff. This results in the development of positive ME-ambient, ME-NP and ME-ET pressure gradients. At times when P_{ME} exceeds P_{ET}, the ET passively opens, gas of ME composition flows from the ME to NP and P_{ME} is reset to the extant value of P_{ET}. The residual ME-Cabin pressure gradient representing the P_{VAS} (i.e. P_{ET} -P_{AMB}) as well as any gradients that develop by transMEM gas exchange (P_{AMB}-P_{ME}-δP_{ME}) or by minor changes in elevation during flight ($P_{AMB}\pm\delta P_{AMB}$-P_{ME}) are reduced by directional gas flows when the ET is actively opened.

On descent, P_{AMB} increases causing increases in P_{NP}, P_{ET} and P_{MEM}, while P_{ME} is relatively unchanged *vis a vis* cruising altitude. This causes a rapidly developing, positive ambient-ME (and ET-ME) pressure gradient, and a relative MEM overpressure with respect to the ME. Under such conditions, neither P_{NP} or P_{ME} will exceed P_{ET} and passive ET openings are

not possible. Consequently, during descent, the passenger must periodically open the ET actively by swallowing to induce mTVP activity or by other maneuvers that cause P_{NP} to transiently exceed the extant P_{ET} or P_{ET} to decrease to less than P_{NP}. Of the latter, Valsalva is the most commonly used wherein air is forcibly expelled from the lungs while keeping the mouth closed and pinching the nose [3, 8, 10, 23, 26]. This greatly increases the P_{NP} which passively opens the ET allowing for NP gas transfer to the ME.

1.1.3 Pathogenesis of Barotrauama

The rapid changes in cabin (ambient) pressure during airplane ascent and descent can overtax the ME pressure-regulating system and provoke barotrauma. For passengers with excellent active ET opening function, ME pressure-regulation during flight is a nominal task; but for those with less efficient ET function, infants and children and those with concurrent nasal inflammation caused by colds or allergy, the task may be impossible [8, 10, 34]. If trans ET gas flow does not adequately buffer the developing ME-ambient pressure gradient during descent, P_{ET} will exert its force over a larger collapsible section of the ET lumen which may then exceed the maximal force exerted by either the mTVP or active NP pressurization [23]. This phenomenon, known as ET "locking", occurs at an individual-specific ME-ambient pressure gradient and effectively obstructs the ET to any further gas flow.

In the absence of adequate pressure-regulation, the large ME-ambient pressure gradients that develop during ascent and descent cause maximal extension of the TM with stretching and tearing of its structural elements. The TM can develop focal hemorrhages, local pocket formation and may perforate [3, 23]. At submaximal extension, this is perceived as a feeling of "fullness" in the ear and at maximal extension as severe pain [2, 35]. These are signs and

symptoms of baromyringitis. Alternatively, at a specified value of approximately 200-300 mmH_2O, the positive P_{AMB}-P_{ME} gradient that develops during descent will cause a large P_{MEM}-P_{ME} gradient resulting in MEM swelling, capillary dilatation, transudative leakage and accumulation of fluid in the ME via "hydrops ex vacuo" [36]. This set of signs presents as barotitis media.

An issue often faced by Otolaryngologists is the assignment of individual patients to risk groups for barotrauma, i.e. which patients can fly safely and which should take precautions prior to airflight [11]. Currently, such assignments are based on history, clinical observations and, in some centers, ET function test results. However, as described in recent reports, these assessments are not useful for many patients and are problematic for patients with existing ME pathologies. In this paper we take a unique approach to addressing this issue by first formulating a mathematical model of ME pressure-regulation during flight based on the physiological considerations outlined above, and then studying the effects on barotrauma of varying the physiological parameters included within the model. The results are used to develop heuristic rules for assigning ears to risk categories for pain, barotitis media and baromyringitis during flight.

1.2 MORPHOMETREIC MODEL OF MIDDLE EAR MUCOSAL GAS EXCHANGE[1]

The middle ear (ME) cleft is a relatively non-collapsible body cavity consisting of an airspace encapsulated by mucosa-covered bone. As depicted in Figure 1.3, the normal ME mucosa is a simple epithelium overlying a thin submucosa interspersed with capillaries. Because the ME

[1] Material in this section used with permission from the Journal of Applied Physiology: 10.1152/japplphysiol.00203.2004

airspace is usually isolated from the ambient environment, transmucosal gas exchange will drive total ME airspace pressure to equilibrium with the summed blood pressures of the physiological gases, a deficit of approximately 50 mmHg when referenced to ambient [37]. Physiologically, that magnitude of underpressure is not realized. There, periodic and transient, muscle assisted openings of the Eustachian tube (ET) allow for gradient driven, bolus exchanges of nasopharyngeal and ME gases that, in turn, reduce the total, preexisting ME-ambient pressure difference. Should ET openings fail to supply a sufficient quantity of gas to balance the volume gas loss by transmucosal exchange, the maximum underpressure is limited by the hydrostatic tissue pressure which, at a relative ME underpressure of approximately 25 mmHg (reference ambient), causes capillary leakage, fluid transudation into the mucosa and the substitution of effusion for air in the ME cavity [38]. This pathological condition, referred to as Otitis media with effusion (OME) impairs the normal transduction function of the ME resulting in a moderate to severe conductive hearing loss [39].

While ET function under normal and pathological conditions has been well studied [13], the demand placed upon the ET for gas resupply is poorly understood [37]. There, because of the relative inaccessibility of the relevant compartments to measurement (e.g. ME mucosa, local blood, ME airspace etc), experiments provide only an indirect measure of transmucosal gas exchange parameters and the resulting data need to be interpreted using mathematical models of the exchange processes [17]. In that regard, the most well developed models are compartmental in nature and require as primary input parameters either direct or indirect measurement of species gas exchange constants. While predictive of ME pressure behavior under a variety of

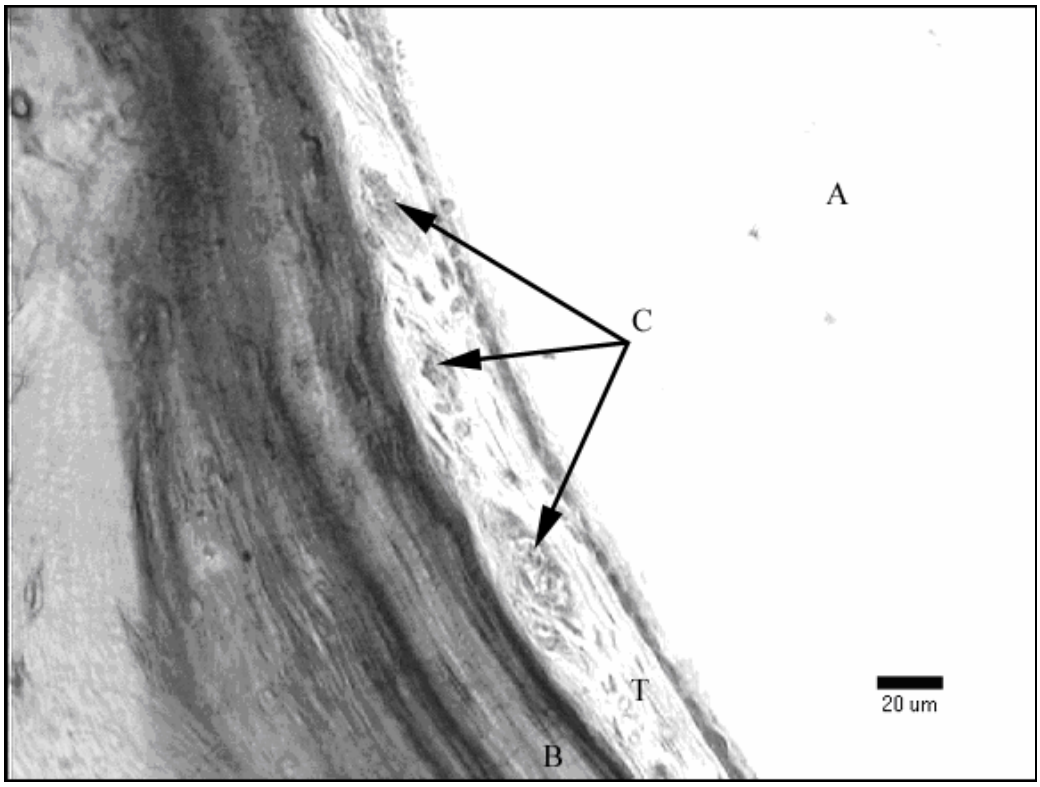

Figure 1.3: Representative histological cross-section of normal human ME mucosa showing the airspace (A), bone (B), capillaries (C) and mucosal tissue (T).

conditions [32, 40, 41], the underlying mechanism(s) must be inferred from agreement between model prediction and experiment, and is not easily related to physiology. Ideally, a complete mathematical model of ME transmucosal gas exchange would require as inputs only the physiochemical properties of the physiological gases (e.g. gas species diffusivity, solubility in tissue/blood etc) and the geometrical relationships for the exchange system (capillary distribution, mucosal thickness, surface area etc). There, the bulk exchange constants used in the compartmental models would be emergent quantities of these more fundamental parameters.

Fink and colleagues [42] recently developed a refinement to these compartmental models, in which they calculated the ME mucosal diffusing capacity (Dm), i.e. the effective barrier resistance to gas flow. This model has the advantage of relying on known physiological

transport parameters and accepted geometrical relations while eliminating the need for artificially constructed parameters. However, their model assumes a constant area-thickness ratio of the mucosal diffusion barrier, calculated from empirical exchange data. Incorporation of measured morphometric parameters into the model geometry would better represent anatomical contributions to the predicted exchange.

A classical approach to modeling air-musosa-capillary gas exchange was developed by Weibel and colleagues [43-45] for the lung. Their method includes a detailed, fine-structure analysis of certain morphometric parameters including diffusional length (τ), which are then used to calculate the mucosal Dm. They treated the pulmonary mucosa as a continuous series of sequential segments that each contribute to Dm, and τ was measured as the harmonic mean of all pathway lengths for each cross-section. A study conducted by Ars and colleagues measured τ [46] within the ME as defined by the linear distance between the air-mucosa boundary and capillary surface. While technically simple to measure, the linear distance measurement assumes that gas exchange occurs along a linear path between blood vessel center of gravity and the air-mucosa interface and, therefore does not account for inhomogeneities in capillary distribution and/or density.

In the present study, we simulated the diffusional fields for a simple geometrical model of the ME mucosa (See Figure 3.1) and evaluated which measure of τ yields a better estimate of the oxygen diffusing capacity (Dm_{O_2}) for the ME. There, Dm_{O_2} was calculated for different model geometries using the two τ measures, linear and harmonic, and the results were compared to predictions from a detailed finite element model (FEM) analysis.

2.0 BAROTRAUMA DURING FLIGHT: PREDICTIONS OF A MATHEMATICAL MODEL

2.1 METHODS

2.1.1 Definition of Disease States

We use the ME-Cabin pressure gradient ($\Delta P_{ME\text{-}Cabin}$) as an index measure of barotrauma, or

$$\Delta P_{ME-Cabin}(t) = P_{ME}(t) - P_{Cabin}(t) \tag{2.1}$$

where P_{ME} and P_{Cabin} are absolute pressures within the ME and cabin at a time step (t). Based on the results of previous studies, we assigned $\Delta P_{ME\text{-}Cabin} \leq$ -250 mmH_2O as the threshold for onset of barotitis media [36] and $|\Delta P_{ME\text{-}Cabin}| \geq$ 1300 mmH_2O as the threshold for onset of baromyringitis with severe pain [8].

2.1.2 Gas Exchange Model

The model compartments and linkages shown in Figure 1.1a depict the gas exchange components of the ME system. All compartments are assumed to be well-mixed and isothermal with inter-compartmental communication defined as the transfer of gas moles down pressure gradients along the linkages. Model compartments include the ME (tympanum + mastoid), MEM, NP, VB and Cabin. The ME is linked periodically to the NP via the ET and continuously with the VB via the MEM. The Cabin acts as the ambient environment for the system, directly

Table 2-I Glossary of terms.

Symbols	*Descriptions*
Pressures	
P_{ME}	Total ME pressure
P_{ME}^{i}	ME partial pressure (O_2, CO_2, N_2, H_2O)
P_{Cabin}	Total Cabin pressure
P_{Cabin}^{i}	Cabin partial pressure (O_2, CO_2, N_2, H_2O)
P_{NP}	Total NP pressure
P_{NP}^{i}	NP partial pressure (O_2, CO_2, N_2, H_2O)
P_{ET}	Tissue pressure surrounding ET lumen
P_{IET}	ET intra-lumen pressure
P_{AMB}	Ambient pressure
P_{VAS}	Vascular pressure
$\Delta P_{ME\text{-}Cabin}$	ME –Cabin pressure differential
$\Delta P_{ME\text{-}NP}$	ME- NP pressure differential
Volumes	
V_{ME}	Middle ear airspace volume
V_{mas}	Mastoid volume
V_{typ}	Tympanum volume
ET passive opening	
$P^{o,}$	ET opening pressure (ref AMB)
$P_{ME\text{-}ET}^{o}$	ME-side opening pressure (absolute)
$P_{ME\text{-}ET}^{o,}$	ME-side opening pressure (ref AMB)
$P_{NP\text{-}ET}^{o}$	NP-side opening pressure (absolute)
$P_{NP\text{-}ET}^{o,}$	ME-side opening pressure (ref AMB)
$P^{c,}$	ET closing pressure (ref AMB)
$A_{ME,}$	ET contact area from ME
$A_{NP,}$	ET contact area from NP
TM displacement	
A_{TM}	TM cross-sectional area
C_{TM}	TM compliance
X_{TM}	TM linear displacement
ET active opening	
F_{ET}	ET “closing” force
F_{ST}	ET Intra-lumen surface tension force
F_{TVP}	Force exerted by mTVP on ET lumen
C_{ET}	ET compliance
X_{ET}	ET mediolateral lumen width
Q_{ET}	transET volume gas flow
R_A	ET active resistance
T_A	ET opening time
S_f	Swallowing frequency
Misc	
k_i	Species specific transMEM exchange time-constants (O_2, CO_2, N_2, H_2O)

affects P_{ET} and $P_{MEM,}$ exerts a mechanical force on the TM, and exchanges gas with the NP and VB. The Cabin is assumed to be an infinite gas source/sink and the volumes of the NP and VB are assumed to be finite but much greater than that of the ME. Consequently, species-gas exchange between the ME and larger compartments does not affect the partial/total pressures of those compartments, but does have a significant effect on ME partial/total pressures.

2.1.3 Cabin Pressurization

During ascent, the airplane rises to a cruising altitude of approximately 30,000 ft above sea level. In order to protect passengers from the adverse affects of the associated extreme, low-pressures, the cabin is pressurized to an effective cruising altitude of approximately 8000 ft [3, 35, 47]. Cabin pressurization was modeled by increasing cabin altitude at a constant rate of 90 m/min (approximately that of a Boeing 747) from departure elevation to the effective cruising altitude [3]. Cabin pressure is a function of cabin elevation and, assuming ideal compressible gas behavior, is given by:

$$P_{Cabin}^{tot}(t) = P_{AMB} e^{\left(\frac{-mgz(t)}{BT_o}\right)}, \tag{2.2}$$

where t is time, g is acceleration due to gravity, m is the average mass of an air molecule, B is boltzman's constant, T_o is the cabin temperature, P_{AMB} is ambient pressure (ref. sea level), and $z(t)$ is the effective altitude of cabin pressurization (ref. sea level). Because gas species mole fractions are constant during flight, cabin N_2 and O_2 partial pressures are calculated using:

$$P_{Cabin}^{N2}(t) = 0.79 P_{Cabin}^{tot}(t), \tag{2.3}$$

$$P_{Cabin}^{O2}(t) = 0.21 P_{Cabin}^{tot}(t). \tag{2.4}$$

Similarly, airplane descent was modeled as a linear decrease from effective cruising to destination altitudes at -90 m/min, while calculating the increases in $P_{Cabin}(t)$.

2.1.4 Pulmonary Exchange

Total NP pressure is assumed to be equal to that of the Cabin or,

$$P_{NP}(t) = P_{Cabin}(t) \ , \tag{2.5}$$

while NP gas species pressures are assumed to be an average of the respective Cabin (experienced during inhalation) and alveolar (experienced during exhalation) values [48]. Total VB pressure is linked to total Cabin pressure via nasopharyngal-pulmonary gas exchange as,

$$P_{VB}(t) = P_{NP}(t). \tag{2.6}$$

Throughout flight, VB partial-pressures of O_2 and CO_2 are assumed to be buffered at constant values by hemoglobin and bicarbonate reactions, the VB remains saturated at a constant H_2O pressure, and VB N_2 pressure is a function of nasopharynygeal N_2 pressure, calculated as:

$$P_{VB}^{N_2}(t) = P_{NP}(t) - P_{VB}^{O_2}(t) - P_{VB}^{CO_2}(t) - P_{VB}^{H_2O}(t). \tag{2.7}$$

2.1.5 Middle Ear Pressure Dynamics during Flight

The driving mechanisms included in the model that affect ME pressure dynamics during flight are transET and transMEM gas exchanges, and the pressure effects of ME volume changes due to TM displacement.

2.1.6 Eustachian Tube Opening

During ET openings, gas flows between the ME and NP in response to the total extant pressure gradient. The ET opens when a force applied to the ET lumen overcomes the ET closing force equal to the sum of the force of the mucosal tissue pressure ($P_{ET}A_{ET}$) and that attributable to intraluminal surface tension (F_{ST}) or:

$$F_{ET}(t) = P_{ET}(t)A_{ET} + F_{ST} \tag{2.8}$$

where A_{ET} is the surface area of mucosal contact.

Pressure-driven ET opening occurs when ME (passive) or NP pressure (active or passive) exerts a force ($P_{ME}A_{ME'}$ or $P_{NP}A_{NP'}$) on the ET lumen greater than F_{ET} such that,

$$P_{ME}(t) > \frac{F_{ET}(t)}{A_{ME'}} = P^{O}_{ME-ET}(t) \quad \text{or} \quad P_{NP}(t) > \frac{F_{ET}(t)}{A_{NP'}} = P^{O}_{NP-ET}(t) \tag{2.9}$$

where $A_{ME'}$ and $A_{NP'}$ are the effective ET surface areas exposed to the ME and NP, respectively, and $P^{O}_{ME\text{-}ET}$ and $P^{O}_{NP\text{-}ET}$ are the ME and NP opening pressures of the ET. These opening pressures have been measured empirically and were reported as pressure differentials referenced to ambient (i.e. $P^{O'}_{ME-ET} = P^{O}_{ME}(t) - P_{AMB}(t)$; $P^{O'}_{NP-ET} = P^{O}_{NP}(t) - P_{AMB}(t)$) [25, 27]. We used representative values from those data sets in this model.

When relative ME overpressures cause the ET to passively open, gas exchange continues until the intraluminal airphase pressure of the ET (P_{IET}) equals the tissue pressure (P_{ET}) of the ET, where $P_{IET} = P_{ME}$. This results in a residual ME overpressure with respect to the NP ($P^{C'}$) that is usually referred to as the ET closing pressure and can be expressed as:

$$P^{C'} = P_{ET}(t) - P_{NP}(t) = P_{VAS}\,. \tag{2.10}$$

Because gas flows from ME to NP, ME species gas fractions are not affected by this transfer and these were calculated by multiplying the preexisting gas fractions by the revised total ME

pressure. As with $P^{O'}_{ME\text{-}ET}$, $P^{C'}$ has been measured empirically [25] and representative values are used in this model.

For ET openings caused by relative NP overpressures, gas exchange first occurs between NP and ME wherein those pressures are equilibrated, and then between ME and NP as ME pressure is reduced to the ET closing pressure. The effect of the NP to ME gas transfers on ME partial pressures at timestep dt was modeled as the weighted average of NP and ME species pressures as given by:

$$\frac{dP^{i}_{ME}(t)}{dt} = y^{i}_{NP}(P^{tot}_{NP}(t) - P^{tot}_{ME}(t)). \tag{2.11}$$

where y_{NP}^{i} equals the species mole fraction in the NP. These partial pressures were then adjusted for the ME to NP gas exchange as described above.

Active muscle-assisted ET opening occurs when the force of mTVP contraction surpasses F_{ET}, where

$$F_{mTVP}(t) > F_{ET}(t). \tag{2.12}$$

For all F_{mTVP} satisfying this condition, the magnitude of that muscular force determines the ET lateral wall displacement as described by Hooke's law:

$$X_{ET}(t) = F_{mTVP}(t)C_{ET}. \tag{2.13}$$

where C_{ET} is the compliance of the ET lumen and X_{ET} is the lumen wall displacement distance. Figure 1.2 provides a detailed representation of the forces acting on the ET during mTVP activity. Assuming that transET gas exchange follows Hagen-Poiseuille flow between two parallel plates [49], then

$$Q_{ET}(t) = \left(\frac{2}{3}\right)\frac{\Delta P_{ME-NP}(t)X_{ET}(t)^{3}W}{\mu L}. \tag{2.14}$$

where: Q_{ET} is the volume of gas transferred, L is the ET length, W is the superior-inferior height of the tube lumen, X_{ET} is the mediolateral lumen width, μ is the viscosity of air and $\Delta P_{ME\text{-}NP}$ is the driving force for transfer. Because W, μ and L are constants for a given ET and X_{ET} is a defined function of F_{mTVP}, we can extract from this equation an analytical expression for the active resistance to gas flow (R_A) that is conditioned on F_{mTVP}, or:

$$R_A(t) = \frac{\Delta P_{ME-NP}(t)}{Q_{ET}(t)} = \left(\frac{3}{2}\right)\frac{\mu L}{W\left(F_{mTVP}(t)C_{ET}\right)^3}. \tag{2.15}$$

While F_{mTVP} is not measurable *in vivo*, R_A is an outcome measure of the forced-response test of ET function which has been used in both clinical evaluations and experimental studies in humans [21, 25, 49, 50]. In the model, R_A is an inputted parameter used to describe mTVP effectiveness with respect to active ET openings with representative values selected from existing data sets. Lacking measured values of F_{mTVP} , we did not include ET "locking" in the model description. We do discuss the implications of this phenomenon in the Discussion section.

Using the empirical measures of R_A and ET opening time (T_A) reported by Cantekin and colleagues [40, 49, 50], transET volume gas exchange can be then be described as the following:

$$Q_{ET}(t) = \frac{\Delta P_{ME-NP}(t)T_A}{R_A}. \tag{2.16}$$

Regular tubal opening by mTVP activity occurs during rhythmic swallowing as reported by Tideholm [51]. In this model, we used a normal swallowing frequency (S_f) of 5.2 openings/hr during cruising and an increased value of 31 openings/hr during descent.

Volume gas flow during mTVP induced tubal openings (at timestep δt) represents the directional movement of a proportional number of gas moles (N) between compartments, with the relationship formalized as:

$$\Delta N_{ET}(\delta t) = \frac{P_{NP}(\delta t) Q_{ET}(\delta t)}{K}\ , \tag{2.17}$$

where K is the product of ME temperature and the gas constant. Assuming an ideal gas, ME pressure after the swallow is calculated from the sum of $\Delta N_{ET}(\delta t)$ and the $N_{ME}(t)$ before the swallow. This value is then used to calculate a new ME volume, $V_{ME}(t+\delta t)$ and ME pressure, $P_{ME}(t+\delta t)$ (see "TM displacement" section below). The effect of these transfers on ME gas species pressures was modeled as described above for the directional transfers caused by passive ET openings.

2.1.7 Middle Ear-Mucosal Gas Exchange

The ME exchanges gas with the local VB by diffusion across the MEM. Here, the MEM was modeled as the VB gas source/sink for this exchange, such that ME gas species pressures, P_{ME}^{i} are calculated as

$$\frac{dP_{ME}^{i}(t)}{dt} = k_i\left(P_{ME}^{i}(t) - P_{VB}^{i}(t)\right), \tag{2.18}$$

where k_i is an empirical species exchange constant, P_{ME}^{i} is ME species pressure, and P_{VB}^{i} is VB species pressure. Equation (18) was applied for N_2, O_2, CO_2 and H_2O and total ME pressure was equal to the summation:

$$P_{ME}^{tot}(t) = \sum P_{ME}^{i}(t)\ . \tag{2.19}$$

Table 2-I lists the initial gas-species pressures for these compartments and the transMEM time-constants measured by experiment [19]. The resultant $P_{ME}(t+\delta t)$ value following transMEM exchange is calculated after the ME volume ($V_{ME}(t+\delta t)$) is adjusted for $\Delta V(t+\delta t)$ (see "TM displacement" section below).

Table 2-II: Initial gas species partial pressure in the ME [18], NP [38], VB and Trans-MEM Exchange Constants [16].

Gas Species	*Partial Pressure (mmHg)*			**Time-Constant**
	ME	**NP**	**VB**	***Rate (min^{-1})***
Oxygen	40	112	45	0.008
Carbon Dioxide	46	32	46	0.16
Water Vapor	47	47	47	0.32
Nitrogen	Balance	Balance	Balance	0.0008

2.1.8 TM Displacement

Figure 1.1c illustrates TM displacements in response to a pressure gradient across the membrane, $\Delta P_{ME\text{-}cabin}$. TM deformation is a function of its compliance and the force applied to the TM (equal to transTM pressure gradient multiplied by TM surface area). The deformation is governed by Hooke's law:

$$X_{TM}(t+\delta t) = \Delta P_{ME-Cabin}(t+\delta t) A_{TM} C_{TM} \tag{2.20}$$

where X_{TM} is the TM displacement distance, A_{TM} is the TM surface area and C_{TM} is the TM compliance. TM volume displacement is calculated as:

$$\Delta V_{TM} = X_{TM}(t+\delta t) A_{TM}, \tag{2.21}$$

with displacements constrained to the range,

$$-\Delta V_{TM}^{\max} < \Delta V_{TM}(t+\delta t) < \Delta V_{TM}^{\max}. \tag{2.22}$$

ME volume is calculated as the sum of the system ME volume and the TM volume displacement as,

$$V_{TM}(t+\delta t) = V_{ME}^{sys} + \Delta V_{TM}(t+\delta t). \tag{2.23}$$

V_{ME}^{sys} is the value of the closed system (i.e. the "initial" starting point for TM displacement calculation), equal to either the initial ME value ($V_{ME}(t=0)$) or the value following the previous

transET or transMEM transfer. From Boyle's Law (i.e. $P_{ME}V_{ME} = \text{constant}$) P_{ME} is then calculated for varying TM displacements, as

$$P_{ME}^{tot}(t+\delta t) = \frac{P_{ME}^{tot}(t)V_{ME}(t)}{V_{ME}(t+\delta t)}. \tag{2.24}$$

Table 2-III: **Average values of model parameters for "normal" MEs used in simulation.**

Parameter	***Description***	***Mean***	***Units***	***Reference***
V_{ME}	ME volume	8.75	mL	[52, 53]
ΔV_{TM}^{max}	TM displacement volume	0.025	mL	[15, 53]
A_{TM}	TM surface area	0.6	cm^2	[54]
κ_{TM}	TM stiffness coefficient	179	mmH_2O/mL	[33]
S_f	Active ET opening rate	5.2	openings/hr	[51]
R_A	ET Active resistance	2	mmHg/cc/min	[49]
T_A	ET active opening duration	0.25	sec	[49]
$P^{O'}_{ME\text{-}ET}$	ME Opening pressure	350	mmH2O	[25]
$P^{O'}_{NP\text{-}ET}$	NP Opening pressure	600	mmH_2O	[27]
$P^{C'}$	Closing pressure	100	mmH_2O	[25]

2.1.9 Simulation Package

The above listed equations allow for the calculation of the time-dependent changes in the ME-ambient pressure gradient during simulated, pressurized flight. The required input parameters for the model are listed in Table 2-II. The relevant equations were coded into a MatLab v.6.1 m-file and entered into a loop which was iterated using a timestep (δt) of 0.001 minutes. Durations of all flights were obtained from published flight schedules, with domestic flights averaging ≈170 minutes in length. The order of sequential operations at each time step was the calculation of: cabin pressurization, gas species-pressures and total pressure for each compartment (P_{Cabin}, P_{NP} and P_{VB}); gas species-pressures and total pressure (P_{ME} adjusted for ΔV_{TM}) for the ME after transMEM exchange, and gas species-pressures and total pressure for the ME after conditional

gas transfers through the ET based on inputted swallowing rhythm (Q_{ET} adjusted for ΔV_{TM}) and/or passive openings (P_{ME} adjusted for ΔV_{TM}).

2.2 RESULTS

2.2.1 Model Validation

To evaluate the predictive accuracy of the model, we simulated the ME pressure dynamics for a pressure chamber experiment by Groth and colleagues [55] who described ME pressure change (measured as TM volume displacements) for pilots exposed to high rates of pressurization (1920 ft/min) over short time periods (25 sec). Model parameters were estimated from the experimental data ($P^{O,}$ = 292 mmH_2O, $P^{C,}$ = 136 mmH_2O , R_A= 7.5 mmHg/cc/min, C_{TM}= 425 mmHg/mL, T_A = 250 msec, and S_f = 33 swallows/ min). A comparison of model and experimental results is shown in Figure 2.1. During ascent, ambient pressure decreased and the resulting ME overpressures caused outward TM displacement. At a relative ME overpressure of 292 mmH_2O, the ET passively opened and the ME-ambient pressure gradient was partly dissipated as gas was transferred from ME to NP, a process interrupted when the ET passively closed at $P_{ME} = P_{ET}$. This was associated with TM repositioning to a lesser volume displacement. During simulated descent, ambient pressure increased causing inward displacement of the TM. At all times, P_{ET} exceeded P_{ME} and P_{NP} and passive ET openings did not occur. Rather, at semi-regular intervals, swallowing caused mTVP contraction and active ET openings. Each opening was associated with a transfer of gas from NP to ME, a consequent reduction in the ME-ambient pressure gradient and reduced TM volume displacement.

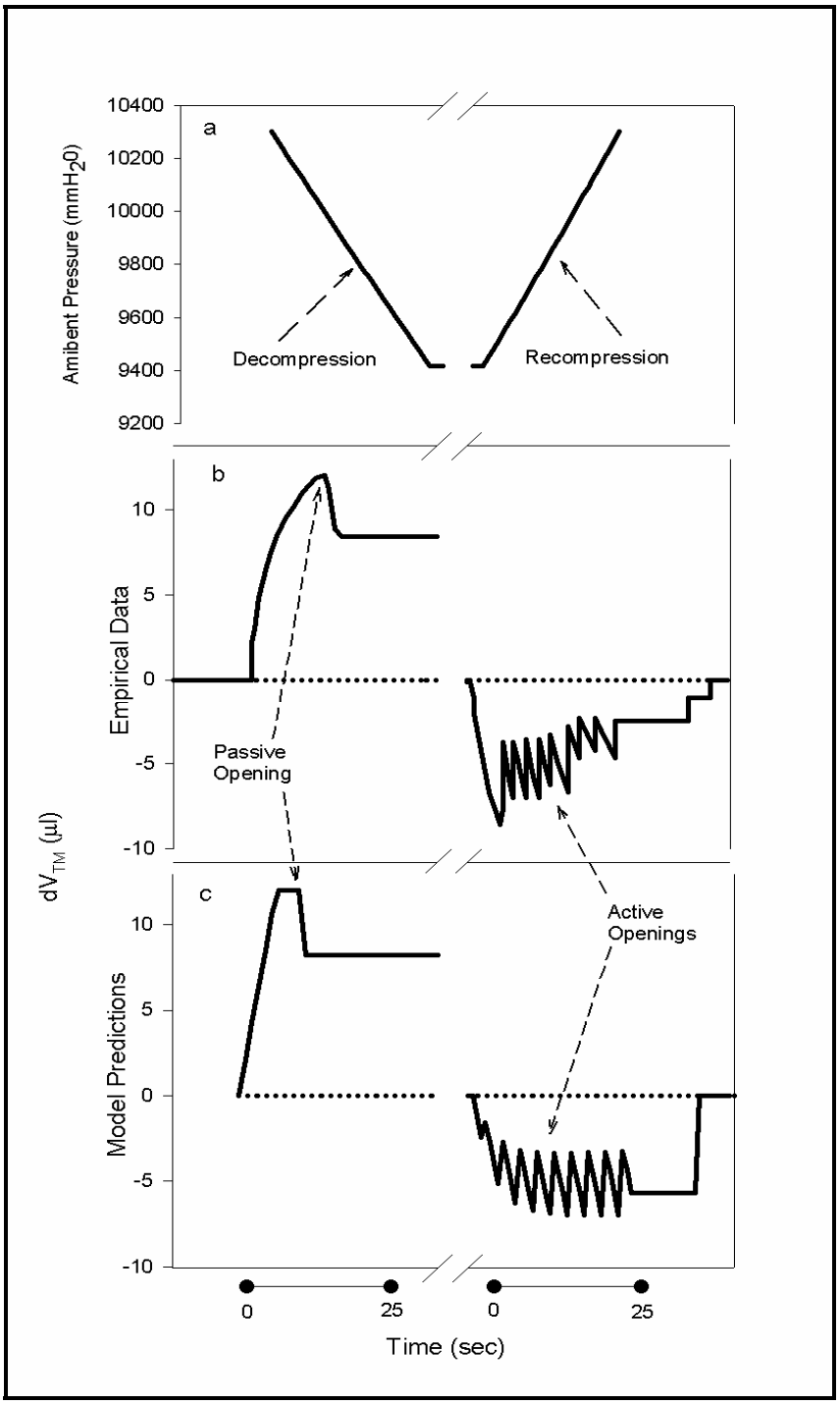

Figure 2.1: Ambient pressure changes for the pressure chamber experiment described by Groth (a), the corresponding experimental TM displacement data for a pilot during compression and decompression (b) and the model predictions for TM displacement (c). Model parameters, fitted to the data were: $P^{O,}$ = 292 mmH_2O, $P^{C'}$ = 136 mmH_2O, R_A= 7.5 mmHg/cc/min, C_{TM}= 425 mmHg/mL, T_A = 250 msec, and S_f = 33 swallows/ min.

Sequential swallows caused a progressive lessening of the residual ME underpressure. This comparison shows that the model accurately predicts and explains experimental ME pressure behavior during simulated flights.

2.2.2 Flight Simulations

Figure 2.2 shows P_{Cabin} as a function of time during three simulated 170 min "flights", each departing from Pittsburgh, PA (PIT) and arriving at: PIT, Denver, CO (DEN) and Miami, FL (MIA). For all "flights", P_{Cabin} decreased during airplane ascent, remained relatively constant during cruising and increased on descent. The magnitude of pressure change experienced by passengers depends on the relative pressure differences between departure/cruising/destination elevations. Table 2-III lists the elevation and ambient pressures for these airports and for the airplane cabin at the effective cruising altitude.

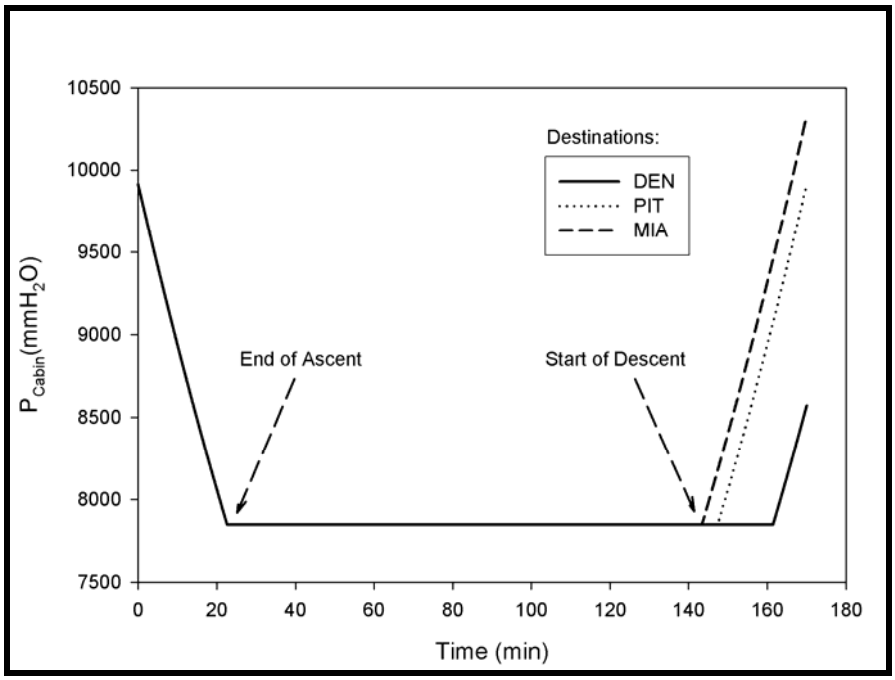

Figure 2.2: Change in P_{Cabin} for 170 minute flights departing from Pittsburgh, PA and arriving at Miami, FL (MIA), Pittsburgh (PIT), and Denver, CO (DEN).

Table 2-IV: Elevations and ambient pressures for airports and airplane cabin [47].

Location	***Elevation (ft)***	***Ambient Pressure (mmHg)***
Pittsburgh, Pa	1204	730
Miami, FL	8	760
Denver, CO	5431	630
London UK	80	758
Location	***Equivalent Elevation (ft)***	***Ambient Pressure (mmHg)***
Airplane Cabin	8000	577

Using these three flight paths, we simulated the ME pressure dynamics for a "normal" ME (See Table 2-II) and for ears with "abnormal" structural (e.g. ME volume, TM displacement) or functional (e.g. $P^{O'}_{ME\text{-}ET}$, R_A) parameters. For example, we simulated flights for MEs with "normal" ET function (Figure 2.3a), a perforated TM (e.g. myringotomy, patent tympanostomy tube) and a patulous ET ($P_{vas}<0$). For all simulated flights, the model yielded the trivial result of a low variance, near zero ("normal" ET function) or continuous zero mmH_2O ME-cabin pressure gradient and consequently protection from barotrauma.

Alternatively, simulations for ears with an ET that fails to open showed flight dependent effects (See Figure 2.3b). There, passive and active pressure driven ET openings were prevented by inputting high $P^{O'}$values ($P^{O'}_{ME\text{-}ET}$ = 2500 mmH_2O, $P^{O'}_{NP\text{-}ET}$ > 2500 mmH_2O) and active, mTVP assisted ET openings were eliminated by inputting a high R_A ($1/R_A \approx 0$). During all ascents, the lack of passive ET openings led to a positive ME-cabin gradient of 2020 mmH_2O, a pressure that exceeds the threshold for pain and baromyringitis. During cruising, that gradient was slightly reduced by the slow, transMEM N_2 exchange, and during descent, the gradient was decreased as P_{Cabin} increased. On landing, the ME-cabin gradient (terminal pressure gradient=TPG) depended almost exclusively on the difference in elevation between departure

and arrival; i.e. the TPG for a flight departing and arriving at PIT was -202 mmH_20, for a flight arriving in DEN was 1070 mmH_20 and for a flight arriving in MIA was -612 mmH_2O, respectively. Only the MIA destination was associated with the expression of barotrauma (barotitis media).

Relaxing the constraint on $P^{O'}$ values ($P^{O'}_{ME\text{-}Tissue}$ =350 mmH2O, $P^{O'}_{NP\text{-}Tissue}$ = 600 mmH_2O) while retaining that for R_A ($1/R_A \approx 0$) simulates a ME whose ET cannot be opened by mTVP activity. Figure 2.3c shows the dynamics of the ME-cabin pressure gradient for the three simulated flights. During ascent, the developing positive ME-cabin pressure gradient is repeatedly reduced to the value of $P^{C'}$ as the ET is passively opened at $P^{O'}$. No barotrauma is experienced during this phase of flight. The residual gradient ($\Delta P_{ME\text{-}Cabin} = P^{C'}$) is slowly reduced during flight by transMEM N_2 exchange. However, the developing negative ME-cabin gradient during descent cannot be alleviated by active, muscle assisted ET openings leading to TPGs of –1731, -2226, and -486 mmH_2O for landings at PIT, MIA and DEN, respectively. All underpressures are of sufficient magnitude to provoke barotitis media and the former two are also expected to provoke baromyringitis.

The results of these simulations are not applicable to ears that are test positive for the Valsalva maneuver (i.e. NP pressure generation > 900 mmH_2O). There, active, pressure-driven inflations of the ME at a sufficient frequency during descent can, like the effect of swallowing maintain near ambient ME pressures, establish near 0 mmH_2O TPGs and prevent barotrauma.

Figure 2.4a shows the simulated ME-cabin pressure gradient during the course of a PIT-MIA flight for an ear with normal and one with compromised mTVP openings (R_A = 2 and 20 mmHg/cc/min; other parameters = “normal” values). The larger value of ET resistance limited transET flow at each opening and led to a sufficiently negative TPG to precipitate barotitis.

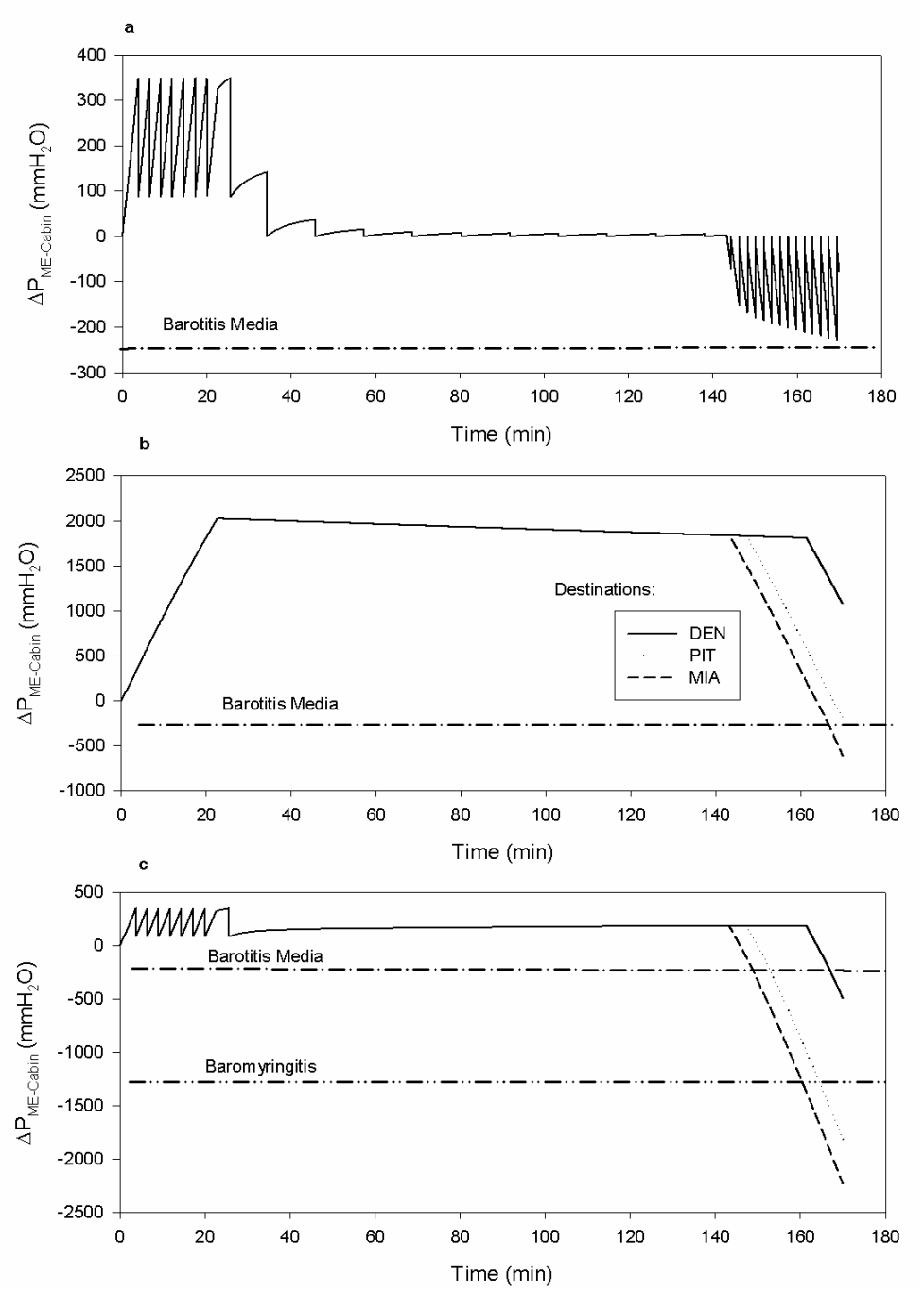

Figure 2.3: Predicted $\Delta P_{ME\text{-}cabin}$ for a "normal" ME with parameters listed in Table 2-II (a), a ME with an obstructed ET ('$P^{O'}_{ME\text{-}Tissue}$ =2500, $P^{O'}_{NP\text{-}Tissue}$>2500 mmH_2O) (b) and a ME unable to actively open the ET ($1/R_A$=0) (c). Barotrauma onset is specified by the dashed indicator lines.

Figure 2.4b shows the simulated ME-cabin pressure gradient for ears with a compromised mTVP assisted ET (R_A = 20 mmHg/cc/min) and two different ME volumes (+/- 50% baseline V_{ME}; other parameters = "normal" values). The smaller ME volume (V_{ME} = 4.4 mL) buffered the effect of the compromised mTVP function on ME-Cabin pressure deviations and prevented the barotitis observed for the large volume ME (V_{ME} = 13.1 mL).

From these observations, the ability to maintain a near zero mmH_2O ME-cabin pressure gradient and thus avoid barotrauma is influenced by the relative magnitudes of volume gas supply and demand. In the absence of active, pressure-driven ET openings, supply is a function of mTVP ET opening efficiency (proportional to $S_f T_A/R_A$) while demand is a function of both the difference in cabin pressure at effective cruising and landing altitudes (maximum ΔP to be equilibrated) and ME volume (moles of gas required to equilibrate that ΔP). Figure 2.5a summarizes this relationship for simulated PIT-MIA flights as a plot of the TPG for ears with constant S_f and T_A but different R_A and V_{ME}. There, low R_A ($\leq$ 4 mmHg/cc/min) allowed for the exchange of sufficient gas volumes to prevent both expressions of barotrauma over all reasonable V_{ME} (< 16mL). Increasing values of R_A protected the ME from barotrauma at lesser and lesser V_{ME} (volume gas demands). As with the limiting case of infinite R_A (see above), the expression of barotrauma can be modified and/or prevented in those ears capable of active, pressure driven ME inflation by Valsalva or other maneuvers.

As noted, the magnitude of ME-ambient pressure deviations in ears with compromised mTVP function can be buffered by TM displacement volume. For a PIT-MIA flight, Figure 2.5b shows the TPG values for a ME with compromised mTVP function (R_A = 8, other parameter values = "normal") as a function of both TM stiffness ($\kappa_{TM}=1/C_{TM}$) and V_{ME} (with $\Delta V_{TM}^{max} \leq$ tympanum

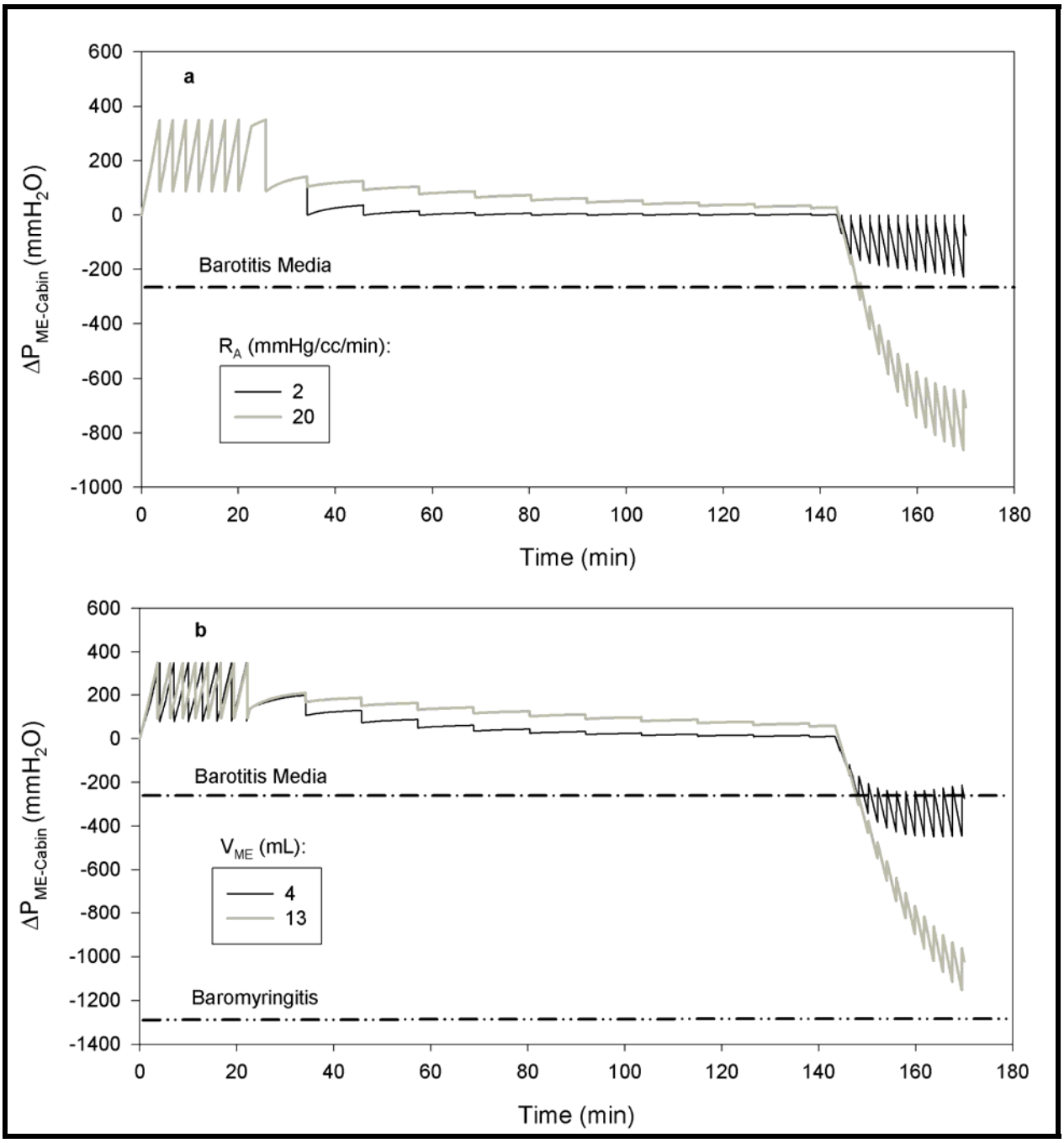

Figure 2.4: $\Delta P_{ME\text{-}cabin}$ as a function of flight time from PIT to MIA for MEs (Table 2-II) with two different R_As and fixed volume = "normal" (a) and for two different volumes at fixed R_A =20mmHg/cc/min (b). Barotrauma onset is designated by the dashed indicator lines. Other parameters were set to "normal".

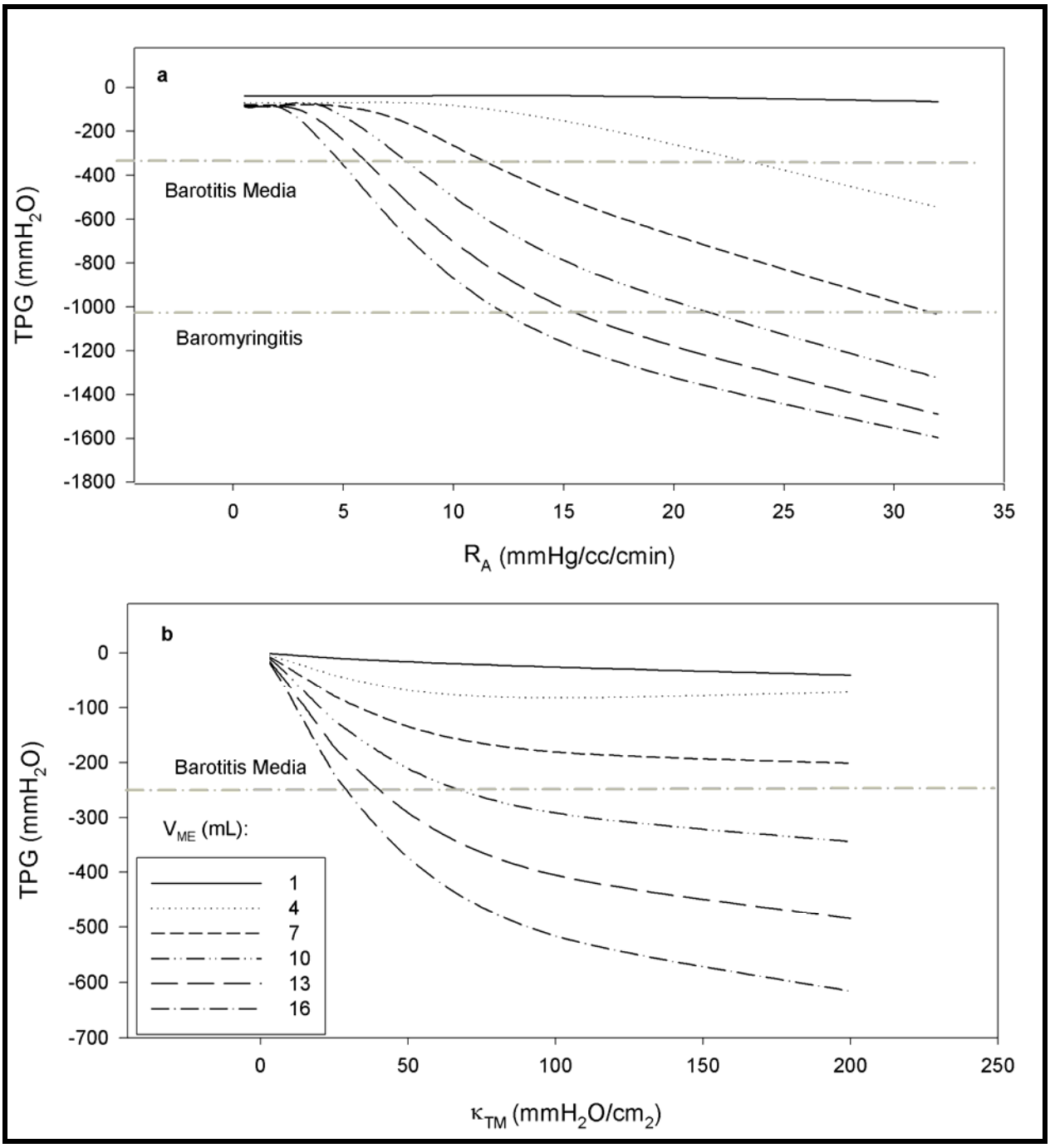

Figure 2.5. PIT-MIA TPG as a function of R_A with fixed TM stiffness coefficient = 179 mmH_2O/mL (a) and as a function of TM stiffness coefficient (κ) with fixed R_A = equal 8 mmHg/cc/min (b) over a range of ME volumes. Barotrauma onset is designated by the dashed indicator lines. S_f was set to 1.1/hr during cruising and 20/hr during descent, other parameters were set to "normal".

volume = 1mL). The plot emphasizes the expected effect of changing the $\Delta V_{TM}/V_{ME}$ ratio on ME-cabin pressure gradients, i.e. greater TPGs at increased TM stiffness and/or greater V_{ME}. Specifically, greater κ_{TM} values were associated with lesser TPG values and the magnitude of this effect was greater for larger V_{ME}. Conversely, hyper-compliant TMs (κ_{TM}< .14 "normal" κ_{TM}) protected the ME from barotitis media over all reasonable V_{ME}. These low values of TM stiffness lie within the range associated with the clinical definition of atelectatic TMs.

Finally, we examined the effect of flight duration on TPG by comparing the predicted TPG values for PIT-MIA (170 min) and PIT to London, UK (533 min), destinations with similar elevations (Table 2-III). For all ME function/structure configurations, the TPGs for the two flights were similar. Because the major difference between these flights is the duration of cruising at fixed altitude, any effect of flight duration will be driven by the rate of transMEM N_2 exchange, a process that was previously measured to be extremely slow.

2.3 DISCUSSION

The model of ME pressure-regulation during flight developed in this report is based on mathematical descriptions of the physiology underlying gas transfers between the ME and adjacent compartments. Calibration of the model parameters was done using published data for disease-free MEs, and thus, this description is not applicable to the ME with Otitis media or Otitis media with effusion. Specifically, those conditions: 1) introduce additional system compartments (e.g. effusion), 2) change the capacitances of existing compartments (e.g. increase MEM volume at the expense of ME volume), and 3) affect the exchange parameters for

transMEM gas transfers (e.g. increase MEM blood flow) [56]. None-the-less, the model does have broad applicability to the "disease free" ME, and to those expressing the predispositions (e.g. poor mTVP function) and/or sequelae (e.g. altered TM compliance, reduced mastoid volume) of those conditions.

Earlier descriptions of barotrauma during airflight usually did not discriminate between barotitis media and baromyringitis in reporting results. As discussed above, these expressions have different underlying causes with the former resulting from a moderate level, positive MEM-ME pressure gradient and the latter resulting from large positive or negative ME-cabin pressure gradients. Consequently, baromyringitis can be experienced throughout flight and is usually associated with signs of TM damage and symptoms of ear-fullness and pain, but barotitis media can only develop during descent, and, in the absence of baromyringitis, is often unrecognized by the traveler. By considering both expressions, our model predicts post-flight ME barotrauma that is and is not perceived by the traveler.

The model results for simulated, flights emphasize the diverse factors that contribute to ME pressure-regulation and underscore the importance of considering contextual relationships in predicting the susceptibility of a given ME to barotrauma. For barotitis media prevention, this concept can be summarized as maintaining a requisite balance in ME gas supply/demand during flight. In this study we have shown that determinate factors of demand (flight elevation changes, ME volume, and TM deformation) are an important aspect of barotrauma development. This is exemplified in our results by the change in ME pressure during "flights" when the ET does not open (no gas supply). While all such ears will have high positive pressures (ref cabin) during cruising and experience baromyringitis, the development of barotitis media on descent will depend on the difference between departure and destination altitudes (demand). A similar

protective effect is provided by high TM volume displacement/ME volume ratios (low demand) and by a patulous ET or a perforated TM (infinite supply). By focusing primarily on the supply side of this balance (ET function), earlier descriptions of the pathogenesis of barotrauma did not included these nuances and, consequently are incomplete [12].

The interactive factors that influence the development of ME barotraumas are organized as an algorithm (Figure 2.6) that provides a systematic method to identify passengers predisposed to barotrauma based on concurrent knowledge of ME anatomy, physiology and flight conditions. The algorithm includes a descending set of more restrictive decision nodes that predict "barotrauma" during flight. The initial two decision-nodes, Non-Intact TM and Patulous ET represent the trivial model solutions of no barotrauma risk for a ME continuously open to the environment. All lower nodes are contextually dependent and require knowledge of the extant relative gas supply/demand balance. For example, Node 3 represents the ability of the mTVP to open the ET along a continuum from excellent to poor. Efficient function eliminates the possibility of barotrauma under all extant conditions while intermediate efficiencies can still protect from barotrama if ME volume is low. Even for ears with poor mTVP function, hyper-compliant TMs can buffer the ME from barotrauma, as can the ability to perform the Valsalva maneuver under specified conditions.

These results show that classifications of ears with respect to barotrauma risk based on clinical observations or simple ET function tests are not accurate [12]. Rather, such assignments require a more complete analysis of the contextual factors that affect ME pressure buffering. A falsifiable test of the predictive accuracy of our model is its ability to explain the accepted observations consistent with as well as those counter-intuitive to the expectations based on the more simple explanations previously advanced. In that regard, our model explains past

observations such as the effects of age and nasal inflammation (concurrent colds or nasal allergy) on the incidence of barotrauma. The age effect is explicable by the established improvement in mTVP functional efficiency (modeled as progressively decreasing R_A) with advancing age [57, 58] and the effect of nasal inflammation is mediated by intraluminal venous engorgement (modeled as a greater P_{ET}) [23]. These explanatory analyses can be extended to include the effects of preventative treatments such as nasal decongestants [23, 59] that act by decreasing tissue inflammation (decreased P_{ET}) or of less well established interventions such as bottle-feeding of infants during descent [34] where the associated jaw movements are believed to initiate mTVP activity (greater S_f) and/or reduce ET tissue pressure (lesser P_{ET}).

A recent publication by Sade [12] reported that patients suffering from "chronic ears" (otitis media with effusion, atelectasis or previously operated cholesteatoma) did not experience barotrauma during flight (by virtue of fewer diagnosed cases) and explained the effect as being mediated by the measured lower volume of the ME resulting from decreased mastoid pneumatization in these ears. There, they argued that the low demand combined with ME-NP gas exchange during active tubal openings allowed for preservation of an ambient ME pressure balance throughout flight and extended this conclusion to the general pediatric population. This conclusion runs contrary to a large amount of previous work showing that active ET function is negligible in ears with concurrent or “at risk” for otitis media with effusion [25, 57, 58, 60]. While our model was not configured to analyze the effects of concurrent disease, component physiological descriptions can be applied to these conditions and the conclusion derived by Sade and colleagues can be examined critically.

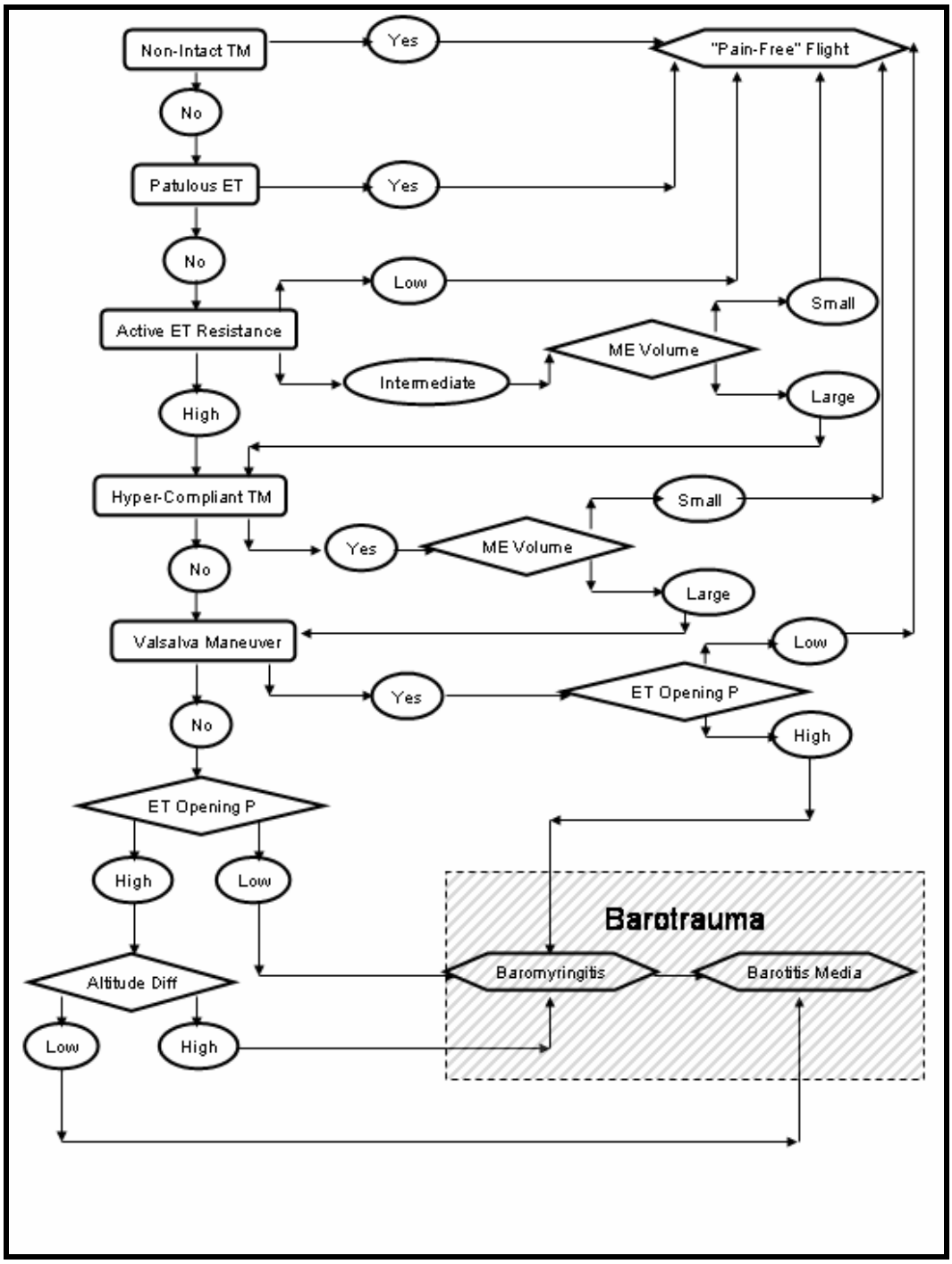

Figure 2.6. Algorithm for determination of a disease-free MEs predisposition to barotrauma. See text for details.

First, ET function tests in "chronic ears" do not demonstrate significantly high opening or closing pressures [25] and thus baromyringitis with pain on ascent is ruled out by the model simulations. Second, those tests do document an inefficient mTVP induced ET opening that, in isolation, should express itself as disease with pain on descent. However, for atelectatic ears, the TM is hyper-compliant and the measured ME volume is small. These conditions increase the TM displacement/ME volume ratio and are expected to buffer the ME-ambient pressure gradient over a wide range of cabin pressures without the need for gas exchange via the ET. In otitis media with effusion, the ME volume is further lessened by the presence of an effusion that effectively limits TM displacements (preventing signs of baromyringitis) and mimics the signs of barotitis. There is no need to propose transET gas exchange to explain the failure to diagnosis barotrauma in ears with preexisting signs. Finally, the cholesteatoma ears were previously operated upon and the concurrent existence (i.e. during the period of air-travel reported) of a condition that initially caused the disease is not prerequisite. We suggest that those ears had a highly compromised ET function preoperatively, but that this subsequently improved to a lesser degree of functional impairment. There the extant, compromised ET function (high R_A) combined with the small ME volume serve to limit the developed pressure gradient on descent with the effect of preventing barotrauma.

3.0 DIFFERENCES BETWEEN TWO METHODS OF MEASURING DIFFUSION LENGTH IN THE PREDICTED OXYGEN DIFFUSING CAPACITY OF THE MIDDLE EAR MUCOSA [2]

3.1 METHODS

We quantified the effect of two τ measures on Dm_{O_2} for different model geometries of the ME mucosa. In brief, one-dimensional Dm_{O_2} was calculated using each of the two τ measures (linear τ_L and harmonic τ_h), and the results were compared to the "true" Dm_{O_2} derived from a detailed, two-dimensional FEM analysis.

3.1.1 Capillary/Mucosa Model Geometry

For quantitative analysis, we chose the simple, yet representative, cross-sectional geometry of the ME mucosa shown in Figure 3.1. Following Weibel and colleagues [43-45], we assume that the ME mucosa is composed of sequentially repeated cross-sections throughout its extent. The exchange system consists of an elliptical capillary which is the only intra-mucosal gas reserve, located within a rectangular section of tissue bounded inferiorly by bone, superiorly by air, and laterally by the field of capillary influence (See Figure 1.3).

[2] Material in this chapter used with permission from the Journal of Applied Physiology: 10.1152/japplphysiol.00203.2004

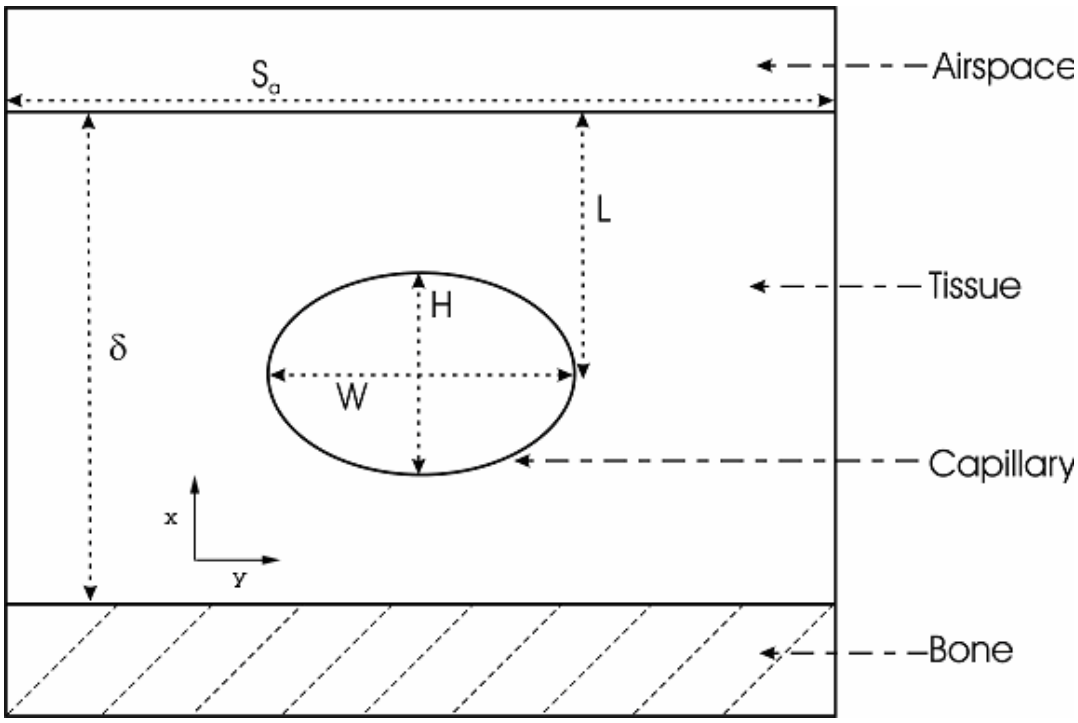

Figure 3.1: Geometry used to model the mucosal cross section (see text for parameter descriptions)

As a first approximation, the model includes only the mucosal barrier to gas diffusion and neglects intra-capillary effects. However, the effect of oxygen uptake by red blood cells on oxygen transport is significant [61, 62], constituting 10-20% of the overall resistance, (see Appendix), and must be included in future model descriptions of macroscopic gas transport.

For a given geometry, the model parameters define variable zones-of-influence for the included capillary that affect gas flux between airspace and capillary. The required inputs for this capillary-mucosa system include: capillary depth, (L), mucosal thickness (δ), mucosal-air interfacial length (S_a) and capillary aspect (width to height) ratio (A_r=W/H). Capillary depth (L) was defined as the distance between capillary centerline and air interface. Mucosal thickness (δ) was defined as the distance from air-mucosa interface to bone. Air-mucosa interfacial length

(S_a) represents the effective surface area per unit depth available for gas exchange within the diffusion system. S_a defines one boundary for the capillary zone of influence and consequently specifies the relative capillary density within tissue. Traditionally, capillary shape is treated as having a circular cross-section, but from qualitative histological analysis of ME tissue we chose to vary capillary cross-section aspect ratio in our model (See Figure 1.3).

Table 3-I: Model parameters.

Symbol	Description	Value	Units
α_{o2}	Oxygen tissue solubility	1.38×10^{-9}	mol mltissue^-1 mmHg^-1
D_{o2}	Oxygen tissue diffusivity at 37 °C	2.81×10^{-5}	cm^2 min^-1
	Specified Partial Pressures		
P_{o2}^{Air}	Air Space O_2	100	mmHg
P_{o2}^{Blood}	Blood-Gas O_2	42	mmHg
	Geometric Parameters	***Mean (μm)***	***Range***
L	Capillary depth (center of gravity)	25	15-65
δ	Mucosal thickness	50	30-80
S_a	Air interface surface area	50	25-75
R	Capillary width	10	10-40
H	Capillary height	10	n/a

With the exception of τ, values of the required morphometric parameters were taken from the data reported for a histological study of the ME mucosa done by Yoon and colleagues [63, See Table 3-I]. Yoon measured ME mucosal thickness in "normal" ears (37.5 +/- 12.5 um) and ears affected by Otitis media with effusion (98 +/- 63.5 um) from which we based our estimate mean (50 um). Yoon also reported capillaries per 100um length tissue (a measure of capillary density within ME mucosa) as 2.00 +/- 0.72 and 4.07 +/- 2.20 in "normal" and OME ears

respectively; which is equivalent to a mean air-mucosa interface length of 50 um. Capillary depth was estimated to fall within the defined tissue section dimensions and aspect ratio was estimated to range from 1 to 4 from qualitative ME mucosa slide observations. Also listed in the table are the physiochemical transport constants used in our simulations as reported by Fink et al. in a ME gas exchange study [42].

3.1.2 One-Dimensional Conductance Model

To describe gas exchange for this simple geometry, we applied a one-dimensional diffusion model that outputs the Dm_{O2} for different model geometries. There, gas exchange within the ME mucosa can be represented as a one-dimensional O_2 flow (Q_{O2}),

$$Q_{O2} = \alpha_{O2} D_{O2} S_a \frac{\Delta P_{O2}}{\tau}, \tag{3.1}$$

The physiochemical parameters, α_{O2} and D_{O2} are mean O_2 solubility and diffusivity in the mucosal tissue (See Table 3-I). Morphometric parameters required to represent the system geometry include S_a and τ. S_a is defined as the effective surface area for gas exchange, which is equivalent to the length of the air-tissue interface given a unit depth of tissue. τ is defined as the distance a gas species must travel along the diffusional path during exchange. The pressure gradient (ΔP_{O2}) is defined as the O_2 pressure difference between ME airspace and local blood, or

$$\Delta P_{O2} = P_{O2}^{air} - P_{O2}^{blood}. \tag{3.2}$$

Dm_{O2} is then given by the lumped transport parameter,

$$Dm_{O2} = \alpha_{O2} D_{O2} \frac{S_a}{\tau}, \tag{3.3}$$

which represents the effective resistance of the mucosa to passive gas exchange as shown in the resulting equation:

$$Q_{O2} = Dm_{O2}\Delta P_{O2}. \tag{3.4}$$

3.1.3 Methods for Morphometric Measurement of Diffusional Length

A cartoon outlining the two methods of measuring τ is presented in Figure 3.2. There, the simple linear measure, τ_l was defined as the distance from the air-mucosa interface to the capillary surface and the harmonic distance measure, τ_h was defined as the harmonic mean of the discrete measurements for the shortest distance between points along the air-mucosa interface and capillary surface.

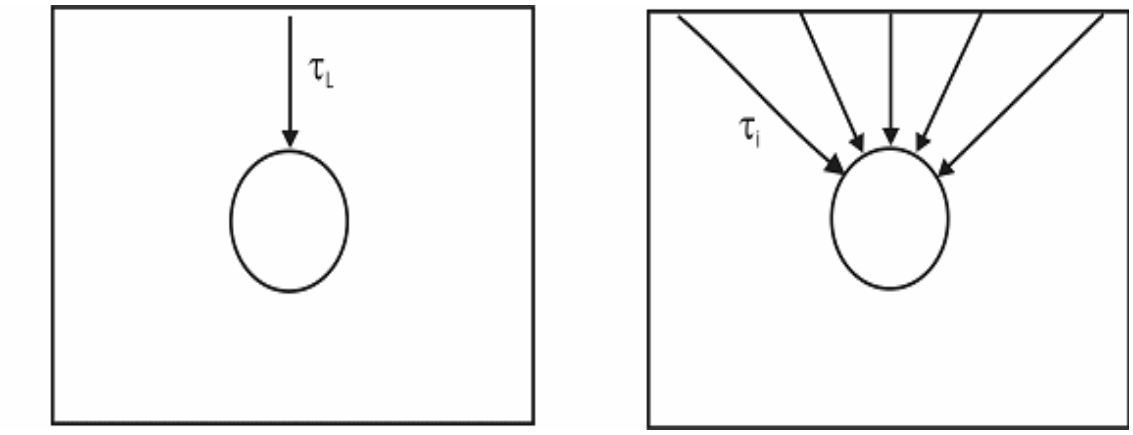

Figure 3.2: Cartoon illustrating the methods for measurement of τ: linear (left) and representative harmonic (right).

For the latter, τ was treated as representing a collection of parallel diffusional pathways, and the inverse of τ_h was approximated by summing the inverse distance measures over the surface length and dividing by the number of measures,

$$\frac{1}{\tau_h} = \frac{1}{n}\sum_{n=1}^{n}\frac{1}{\tau_i}. \tag{3.5}$$

This calculation places greater weight on the shorter interface-capillary paths which is expected to better represent local gas exchange. Each of the two measures was calculated for the different model geometries and the results were used to estimate the respective Dm_{O2} values for those geometries: Dm_{O2}^{L} and Dm_{O2}^{h}.

3.1.4 Finite Element Analysis

Earlier studies used FEM to calculate Dm for the pulmonary mucosa [64, 65]. We used a similar FEM method to describe the two-dimensional ME gas exchange system. This model utilizes the governing steady-state diffusion equation,

$$\nabla^2 P_{O2} = 0, \tag{3.6}$$

where $\nabla^2\left(=\frac{\partial^2}{\partial x^2}+\frac{\partial^2}{\partial y^2}\right)$ is the laplacian operator and PO2 is oxygen partial pressure. We assume that oxygen exchange is primarily diffusion-limited in that mucosal blood perfusion does not significantly affect local tissue partial pressure. While this assumption is supported by previous work that analyzed the contribution of convection to pulmonary gas flux [61, 62], it is included here to simplify our initial simulations and will be relaxed in later model enhancements. Gas exchange within mucosal tissue is driven by the extant pressure gradients between local blood at the capillary surface ($P_{O2} = P_{O2}^{blood}$) and the ME air space ($P_{O2} = P_{O2}^{air}$) specified at the

boundary condition. Because of the negligible gas diffusivity in bone that boundary is treated as a no-flux condition: $\left.\frac{\partial P_{O2}}{\partial x}\right|_{x=\delta} = 0$. Since the tissue cross-section is defined as the complete zone of influence for the modeled capillary, all significant blood-tissue gas exchanges occur within the modeled region and the lateral tissue boundaries are specified as no-flux positions: $\left.\frac{\partial P_{O2}}{\partial y}\right|_{y=\left(\frac{+}{-}\right)\frac{S_a}{2}} = 0$.

In the FEM analysis, the governing diffusive gas transport equation was solved using the computational software package FEMLAB (version 2.3.0.145). First, for the model geometry, a wireframe mesh network was generated which placed nodes throughout the region of interest (see Figure 3.3a). Next, species partial pressure was solved at node interfaces. The mesh was refined until the computational simulation was independent of the number of elements/nodes (1532 nodes for our baseline geometry). Total Q_{O2} was determined by integrating flows normal to the air-mucosa interface:

$$\mathrm{Q}_{O2} = \int_s \alpha_{O2} \mathrm{D}_{O2} \left.\frac{\partial P_{O2}}{\partial x}\right|_{\text{interface}} \partial s \qquad (3.7),$$

where the $\frac{\partial P_{O2}}{\partial x}$ is evaluated over the interface. The effective Dm_{O2}' is then specified as

$$Dm'_{O2} = \frac{\mathrm{Q}_{O2}}{\Delta P_{O2}} \qquad (3.8),$$

which was accepted as the "true" value of that parameter for all model simulations.

3.2 RESULTS

The O_2 flux fields predicted for different ME geometries by FEM analysis are shown in Figure 3.3b-d; flux vectors point in the direction of transport and vector length is proportional to flux magnitude. The baseline cross-section (b) contains a centrally located, circular capillary. O_2 flux within the tissue is perpendicular to the air-mucosa interface most proximal to the capillary with very little contribution from more distal regions of the interface. The effect of changing the capillary aspect ratio and capillary depth on the O_2 flux field is shown in Figure 3.3c and d, respectively. For both of these extreme conditions, O_2 flux is relatively linear and perpendicular to the air-mucosa interface.

The impact on Dm_{O2}' of changing the values for each geometrical parameter was quantified using a sensitivity analysis. There, each model parameter was adjusted to +50% of the baseline value and the percent change in Dm_{O2}' was determined. As expected, Dm_{O2}' was independent of mucosal thickness (Dm_{O2}' <1%), but was dependent on those parameters that inherently contribute to the diffusional pathways: i.e. capillary depth (Dm_{O2}' ≈46%), capillary aspect ratio (Dm_{O2}'≈13%) and air-mucosa interface length (Dm_{O2}' ≈19%).

The effect of varying capillary depth on Dm_{O2}', Dm_{O2}^{L} and Dm_{O2}^{h} is shown in Figure 3.4a. Differences between Dm_{O2}' and each of the morphometric estimates are large at small capillary depths (e.g. L of 15: Dm_{O2}^{L} 76.4% difference and Dm_{O2}^{h} 26.3% difference), but are less at large capillary depths (e.g. L of 65um: Dm_{O2}^{L} 13.4% difference and Dm_{O2}^{h} 10.8% difference). This effect of capillary depth on estimate deviation is explicable by the non-uniform diffusion fronts that develop for small depths which cause heterogeneous, proximal to distal decreases in gas flux along the air-tissue interface. In contrast, for larger capillary depths, more uniform

diffusion fronts develop allowing for more homogeneous gas flux across the entire air-mucosa interface, an assumption made in the morphometric models. Note that for all capillary depths, the estimate provided by $Dm_{O_2}{}^{L}$ more poorly represents the respective Dm_{O_2}' when compared to the $Dm_{O_2}{}^{h}$ estimate showing that the latter captures more complete information with respect to system geometry.

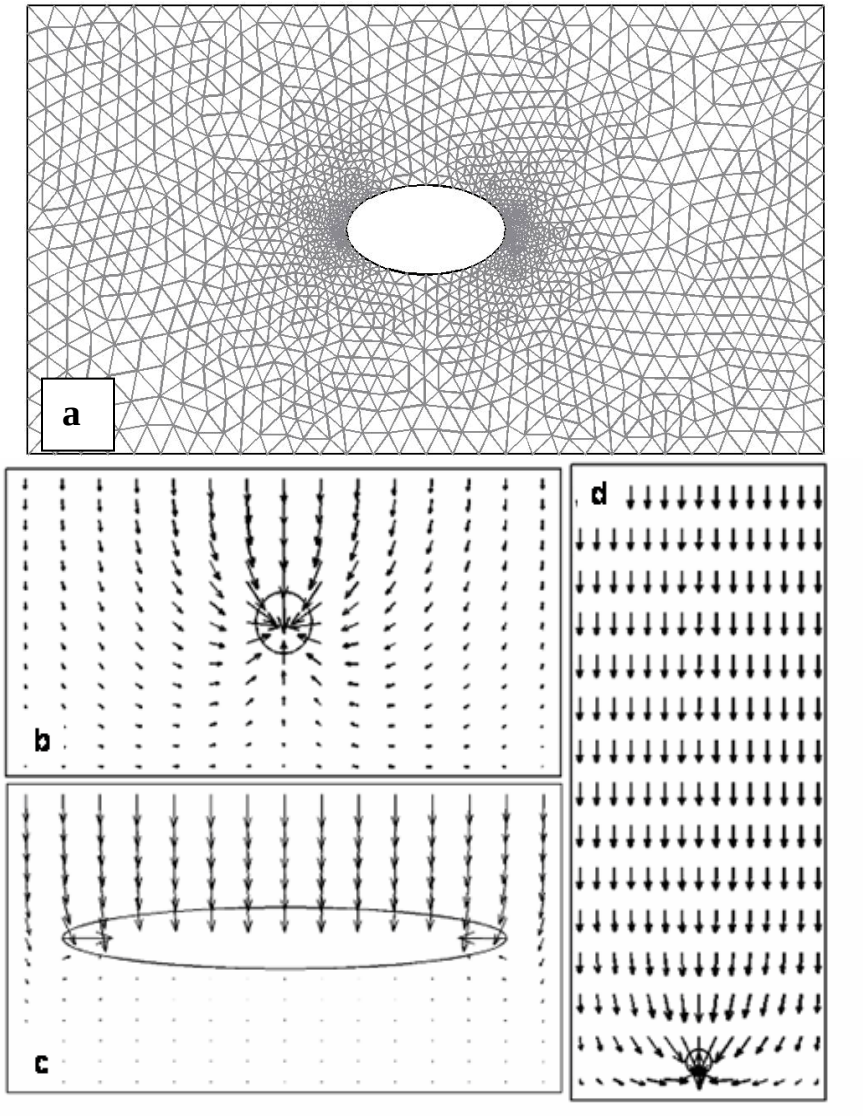

Figure 3.3: a) Finite element mesh network used for detailed analysis of gas flux, and the corresponding O2 diffusion fields predicted by FEM analysis and the corresponding O_2 diffusion fields predicted by FEM analysis for b) (upper left) a basal condition, c) (lower left) increased capillary aspect ratio and d) (right) larger capillary depth.

The effect on the three Dm_{O2}' estimates of varying capillary aspect ratio over the range from 1 to 4 is shown in Figure 3.4b. Based on qualitative, histological study of ME mucosal specimens that demonstrate orientation of the capillary "long axis" along the width parameter, we chose to model this geometry by maintaining a constant height and varying capillary width. Because the τ_L measure does not incorporate variance in capillary shape, $Dm_{O2}{}^{L}$ was independent of A_r. Deviation between Dm_{O2}' and $Dm_{O2}{}^{h}$ was less than that between Dm_{O2}' and $Dm_{O2}{}^{L}$ over all A_r. This effect is explicable by the heterogeneous diffusion fronts present for circular capillaries where flux contributions decrease progressively from more distal regions of the air-mucosa interface, a property more accurately captured by the τ_h measure. However, our results show that Ar was not a dominant factor in Dm_{O2} classification, with $Dm_{O2}{}^{h}$ prediction only varying ≈10% from a 400% increase in A_r. This result allows us to conclude that A_r is not a geometrical characteristic important to gas exchange and gives us confidence that artifacts in capillary shape resulting from oblique slicing would not introduce significant errors.

The effect of varying tissue-air interface length on the three estimates of Dm_{O2} is shown in Figure 3.4c. Lesser deviations between Dm_{O2}' and both $Dm_{O2}{}^{L}$ and $Dm_{O2}{}^{h}$ are evident at smaller lengths (S_a of 25um: $Dm_{O2}{}^{L}$ 13.36% difference and $Dm_{O2}{}^{h}$ 8.32% difference) when compared to the more pronounced deviations at larger lengths (S_a of 75: $Dm_{O2}{}^{L}$ 73.4% difference and $Dm_{O2}{}^{h}$ 32.9% difference). Larger air-mucosa interfaces (per capillary) reflect lower capillary density whereas smaller interfaces represent more uniform capillary distributions throughout the mucosa. This relationship respectively mimics the effects of the high and low A_r on flux fields as discussed above. As with the other simulated geometries, better agreement between the derived Dm_{O2} estimates and Dm_{O2}' is achieved using the τ_h measure.

3.3 DISCUSSION

A fundamental, mathematical description of transmucosal gas exchange for the normal and diseased ME can be used to explain the mechanism underlying the development and persistence of Otitis media with effusion, as well as to suggest options for the targeted treatment of that disease [37]. Compartmental exchange models are not mechanistically determinant and therefore cannot be used for those purposes. This limitation can be avoided using morphometric models that include fine structure details of parameters known to influence gas exchange between the ME airspace and mucosal capillary [17]. In modeling gas exchange for the lung, the required morphometric parameters for accurate representation of physiology included tissue volume, capillary distribution and the surface areas for the exchange unit [43-45]. That approach requires first determining the effective τ for a given geometry which is then used to generate the diffusional properties for specified mucosal geometries [43-45]. Here, we used a modification of that approach to model transmucosal gas exchange for the ME [46].

When used as morphometric model inputs, measurement of all relevant geometrical parameters for all ME regions and under all mucosal conditions (e.g. age, disease state etc.) is expected to yield results that accurately predict ME transmucosal gas exchange for the normal and diseased mucosa. However, such an approach is not technically feasible. Consequently, a first priority for model development is the definition of a measurement subset that captures the information most important to system dynamics as reflected by predictive accuracy. One parameter known to be a member of that subset is τ which represents the effective length of the diffusion pathway between air-mucosa interface and capillary.

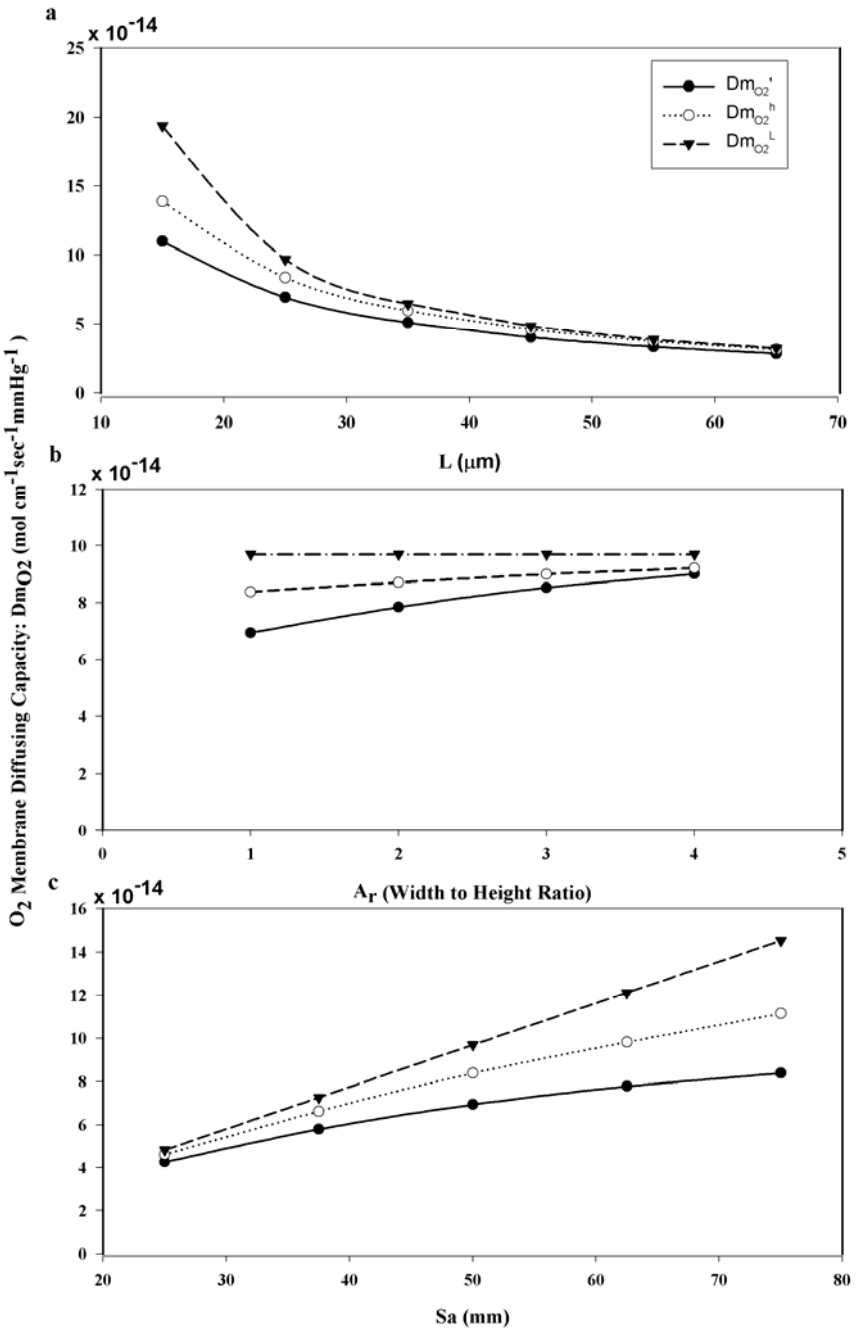

Figure 3.4: Predicted mucosal diffusion capacitance as a function of a) capillary depth, b) capillary aspect ratio, and c) tissue-air interface length for the three estimation methods.

In this study, we compared two relatively easy techniques for measuring τ with respect to their ability to generate Dm_{O_2} sets for different ME mucosal geometries that are consistent with

the respective set generated using a more complex FEM approach where τ is not an input parameter [43, 44, 46, 64-66]. The results showed that the τ defined by the harmonic mean distance better represents the Dm_{O2} for the FEM analysis. This predictive improvement is attributable to the fact that, unlike the linear measure, the harmonic mean measure incorporates information related to capillary shape and density.

None-the-less, neither one-dimensional, morphometric model accurately represented the Dm_{O2} set predicted by the FEM analysis. The morphometric estimates predicted Dm_{O2} appropriately in some instances (large L, large A_r, and small S_a), but erroneously in others (small L, small A_r, and large S_a). These simple models overestimated the Dm_{O2}' (positive bias) and the magnitude of the error varied with extant conditions (non-linear bias). This exposes limitations of even our better one-dimensional model for ME transmucosal gas exchange and shows that results from such simulations cannot be used to accurately predict the continuum of change in gas exchange behavior from the normal to pathological mucosa. Because of these listed errors, we question the applicability of a morphometric approach to estimating geometrical parameters within this specific exchange system: the ME mucosa.

Wiebel's successful formulation of pulmonary gas exchange using a morphometric model led us to a similar approach for describing ME transmucosal gas exchange [43-45]. However, as evidenced by the comparative simulations reported here, we adopted a cautious, stepwise approach that first explored the adequacy of the morphometric model to accurately represent system behavior. There, we recognized that there are significant differences in the fine-structure of the exchange system for the lung and ME. For example, alveolar walls are thin tissue structures, embedded with capillaries, and symmetrically bounded by airspace. Gas exchange

within this geometry can be described using symmetry, with capillary surfaces proximal to air interface boundaries specified as the "active" sites for airspace-mucosa-capillary gas exchange. However, this simplifying assumption fails for the ME mucosal geometry where bone opposes the basal mucosal surface allowing the entire capillary surface to participate in mucosa-blood exchange with a single air interface (See Figure 3.3b). Also, the flux fields generated by FEM analysis document curvilinear diffusional paths, an effect not reproduced in the morphometric models which assume linear species transport and contributions from the total available surface area. A similar discrepancy between the results for red blood cell diffusing capacity in pulmonary capillaries generated by morphometric models and FEM analysis was noted by Hsia and colleagues [64, 66]. There, morphometric models contained "fundamental oversimplifications", unable to account for factors found important to gas exchange. These and other differences in pulmonary/ME mucosal geometry may explain the failure of the morphometric models developed for the lung to accurately represent the Dm_{O2} for the ME mucosa.

4.0 SUMMARY

4.1 BAROTRAUMA DEVELOPMENT DURING AIRPLANE FLIGHT

In conclusion, we present a physiological model of barotrauma development in "disease-free" MEs during flight. The presented model accommodates previous observations and can explain observations that are unexpected using previous descriptions based exclusively on ET function. Modifications of model parameters can give insights into prophylactic treatment possibilities with a high likelihood of preventing barotrauma. As inputs, the model requires measurement of a number of parameters not usually obtained in the clinical setting (e.g. ME volume, transMEM gas exchange constants, TM volume displacement, R_A etc.) and this requires invasive tests (e.g. myringotomy). For the occasional air-traveler, these assessments may not be warranted, but this is not true for professionals (e.g. cabin crews, military pilots etc) who fly regularly.

4.1.1 Future Work

Currently, we are generalizing the model to include the effects of concurrent ME disease expressions. We also hope to compare individual-specific model predictions to empirical data derived from pressure chamber tests.

4.2 MORPHOMETRIC MODEL OF MIDDLE EAR GAS EXCHANGE[3]

Here, oxygen diffusing capacity was calculated for different ME mucosal geometries using the two τ measures, and the results were compared to those predicted by a detailed, 2-dimensional finite element analysis. Predictive accuracy was improved by incorporating the τ measure described by Weibel which captures important information regarding variations in capillary shape and distribution. However, when compared to the oxygen diffusing capacity derived from the finite element analysis, both measures yielded non-linear, positively biased estimates. The morphometric techniques underestimate diffusion length by failing to account for the curvilinear gas flow pathways predicted by the finite element model.

4.2.1 Future Work

Results of this study question the capability of the model to properly predict diffusing capacity across the continuum of normal to inflamed (pathologic) states. An investigation to determine the capability of the model to predict physiological exchange occurring in both states is underway.

[3] Material in this section used with permission from the Journal of Applied Physiology: 10.1152/japplphysiol.00203.2004

5.0 APPENDIX[4]

5.1 APPROXIMATION OF INTRA-CAPILLARY OXYGEN DIFFUSING CAPACITY

Inclusion of intra-capillary gas transport within calculation of the *total* diffusive capacitance is defined as,

$$\frac{1}{DL_{O2}} = \frac{1}{Dm_{O2}} + \frac{1}{\Theta V_c}, \tag{2.9}$$

where DL_{O2} is the total oxygen diffusing capacity, Dm_{O2} is the membrane component, Θ is the rate of oxygen binding in whole blood (per time) and V_c is the total capillary volume. From this we approximated the percentage contribution of membrane and intra-capillary components to total diffusive capacitance for our model baseline geometry. We calculated the membrane component of oxygen diffusing capacity ($Dm_{O2} = 6.95 \times 10^{-14}$ $molO_2$ sec^{-1} $mmHG^{-1}$) from values in Table 3-I. For the reactive uptake component we multiplied the baseline geometry capillary volume ($V_c = 4.85 \times 10^{-7}$ cm^2) by published estimates for oxygen uptake rate (Θ) [67]. Table 5-I shows the percent resistance attributable to each component of diffusive capacitance for each Θ estimate. This brief analysis shows that the membrane component is the dominant controlling factor to total diffusive capacitance but intra-capillary resistance remains an important aspect by contributing approximately 10-20%.

[4] Material in this chapter used with permission from the Journal of Applied Physiology: 10.1152/japplphysiol.00203.2004

Table 5-I: Analysis of membrane and intra-capillary component contribution to total diffusive capacitance. With Θ values reported in ($molO_2\ sec^{-1}mL^{-1}\ mmHG^{-1}$) and DL_{O2} values reported in ($molO_2\ sec^{-1}\ mmHG^{-1}$).

Θ Estimate source	Θ Values (x 10^7)	DL_{O2}(x 10^{14})	Intra-capillary % Contribution	Membrane % Contribution
Roughton / Forster	6.85	6.15	11.44	88.56
Holland	4.84	5.87	15.46	84.54
Forster	4.45	5.79	16.60	83.40

BIBLIOGRAPHY

1. Stangerup, S.E., et al., *Barotitis in children after aviation; prevalence and treatment with Otovent.* J Laryngol Otol, 1996. **110**(7): p. 625-8.

2. Devine, J.A., et al., *The use of tympanometry to detect aerotitis media in hypobaric chamber operations.* Aviat Space Environ Med, 1990. **61**(3): p. 251-5.

3. Parris, C. and S. Frenkiel, *Effects and management of barometric change on cavities in the head and neck.* J Otolaryngol, 1995. **24**(1): p. 46-50.

4. Becker, G.D. and G.J. Parell, *Barotrauma of the ears and sinuses after scuba diving.* Eur Arch Otorhinolaryngol, 2001. **258**(4): p. 159-63.

5. Fitzpatrick, D.T., et al., *Risk factors for symptomatic otic and sinus barotrauma in a multiplace hyperbaric chamber.* Undersea Hyperb Med, 1999. **26**(4): p. 243-7.

6. Miyazawa, T., H. Ueda, and N. Yanagita, *Eustachian tube function and middle ear barotrauma associated with extremes in atmospheric pressure.* Ann Otol Rhinol Laryngol, 1996. **105**(11): p. 887-92.

7. Hamilton-Farrell, M. and A. Bhattacharyya, *Barotrauma.* Injury, 2004. **35**(4): p. 359-70.

8. Brown, T.P., *Middle ear symptoms while flying. Ways to prevent a severe outcome.* Postgrad Med, 1994. **96**(2): p. 135-7, 141-2.

9. Armstrong, H. and J. Heim, *The effect of flight on the middle ear.* J.A.M.A., 1934. **109**(6): p. 417-421.

10. Hanna, H.H., *Aeromedical aspects of otolaryngology.* Aviat Space Environ Med, 1979. **50**(3): p. 280-3.

11. Weiss, M.H. and J.O. Frost, *May children with otitis media with effusion safely fly?* Clin Pediatr (Phila), 1987. **26**(11): p. 567-8.

12. Sade, J., A. Ar, and C. Fuchs, *Barotrauma vis-a-vis the "chronic otitis media syndrome": two conditions with middle ear gas deficiency Is secretory otitis media a contraindication to air travel?* Ann Otol Rhinol Laryngol, 2003. **112**(3): p. 230-5.

13. Bluestone, C.D. and W.J. Doyle, *Anatomy and physiology of eustachian tube and middle ear related to otitis media.* J Allergy Clin Immunol, 1988. **81**(5 Pt 2): p. 997-1003.

14. Isono, M., et al., *Computerized assessment of the mastoid air cell system.* Auris Nasus Larynx, 1999. **26**(2): p. 139-45.

15. Sade, J., *The buffering effect of middle ear negative pressure by retraction of the pars tensa.* Am J Otol, 2000. **21**(1): p. 20-3.

16. Doyle, W.J., et al., *Exchange rates of gases across the tympanic membrane in rhesus monkeys.* Acta Otolaryngol, 1998. **118**(4): p. 567-73.

17. Doyle, W.J., *Mathematical model explaining the sources of error in certain estimates of the gas exchange constants for the middle ear.* Ann Otol Rhinol Laryngol, 2000. **109**(6): p. 533-41.

18. Felding, J.U., J.B. Rasmussen, and T. Lildholdt, *Gas composition of the normal and the ventilated middle ear cavity.* Scand J Clin Lab Invest Suppl, 1987. **186**: p. 31-41.

19. Doyle, W.J., J.T. Seroky, and C.M. Alper, *Gas exchange across the middle ear mucosa in monkeys. Estimation of exchange rate.* Arch Otolaryngol Head Neck Surg, 1995. **121**(8): p. 887-92.

20. Doyle, W.J., C.M. Alper, and J.T. Seroky, *Trans-mucosal inert gas exchange constants for the monkey middle ear.* Auris Nasus Larynx, 1999. **26**(1): p. 5-12.

21. Elner, A., *Normal gas exchange in the human middle ear.* Ann Otol Rhinol Laryngol, 1976. **85**(2 Suppl 25 Pt 2): p. 161-4.

22. Swarts, J.D. and S.R. Rood, *The morphometry and three-dimensional structure of the adult eustachian tube: implications for function.* Cleft Palate J, 1990. **27**(4): p. 374-81.

23. Dickson, E.D.D., J.E.G. McGibbon, and A.C.P. Campbell, *Acute Otitic Barotrauma - Clinical findings, mechanism and relationship to the pathological changes produced experimentally in the middle ears of cats by variations in pressure.* J Laryngol Otol, 1943.

24. Ghadiali, S.N., J. Banks, and J.D. Swarts, *Effect of surface tension and surfactant administration on Eustachian tube mechanics.* J Appl Physiol, 2002. **93**(3): p. 1007-14.

25. Swarts, J.D. and C.D. Bluestone, *Eustachian tube function in older children and adults with persistent otitis media.* Int J Pediatr Otorhinolaryngol, 2003. **67**(8): p. 853-9.

26. Ingelstedt, S., *Physiology of the Eustachian tube.* Ann Otol Rhinol Laryngol, 1976. **85**(2 Suppl 25 Pt 2): p. 156-60.

27. Chan, K.H., et al., *Autoinflation of eustachian tube in young children.* Laryngoscope, 1987. **97**(6): p. 668-74.

28. Ghadiali, S.N., J. Banks, and J.D. Swarts, *Finite Element Analysis of Active Eustachian Tube Function.* J Appl Physiol, 2004.

29. Hamada, Y., H. Utahashi, and K. Aoki, *Physiological gas exchange in the middle ear cavity.* Int J Pediatr Otorhinolaryngol, 2002. **64**(1): p. 41-9.

30. Mover-Lev, H., et al., *Quantitative analysis of gas losses and gains in the middle ear.* Respir Physiol, 1998. **114**(2): p. 143-51.

31. Sade, J., *On the function of the pars flaccida: retraction of the pars flaccida and buffering of negative middle ear pressure.* Acta Otolaryngol, 1997. **117**(2): p. 289-92.

32. Doyle, W.J., *Mucosal surface area determines the middle ear pressure response following establishment of sniff-induced underpressures.* Acta Otolaryngol, 1999. **119**(6): p. 695-702.

33. Gaihede, M., T. Lildholdt, and J. Lunding, *Sequelae of secretory otitis media: changes in middle ear biomechanics.* Acta Otolaryngol, 1997. **117**(3): p. 382-9.

34. Byers, P.H., *Infant crying during aircraft descent.* Nurs Res, 1986. **35**(5): p. 260-2.

35. Westerman, S.T., M.B. Fine, and L. Gilbert, *Aerotitis: cause, prevention, and treatment.* J Am Osteopath Assoc, 1990. **90**(10): p. 926-8.

36. Swarts, J.D., et al., *In vivo observation with magnetic resonance imaging of middle ear effusion in response to experimental underpressures.* Ann Otol Rhinol Laryngol, 1995. **104**(7): p. 522-8.

37. Doyle, W., *Middle ear pressure regulation. The Function and Mechanics of Normal, Diseased and Reconstructed Middle Ears.*, in *The Hague*, J.R.a.S. Merchant, Editor. 2000, Kugler Publications: Netherlands. p. 3-21.

38. Alper, C.M., et al., *Magnetic resonance imaging of the development of otitis media with effusion caused by functional obstruction of the eustachian tube.* Ann Otol Rhinol Laryngol, 1997. **106**(5): p. 422-31.

39. Bluestone, C.D. and J.O. Klein, *Otitis media in infants and children*. 3rd ed. 2001, Philadelphia: W. B. Saunders. 404 , [2] of col. plates.

40. Cantekin, E.I., et al., *Normal and abnormal middle ear ventilation.* Ann Otol Rhinol Laryngol Suppl, 1977. **86**(4 Pt 3 Suppl 41): p. 1-15.

41. Doyle, W.J. and C.M. Alper, *A model to explain the rapid pressure decrease after air-inflation of diseased middle ears.* Laryngoscope, 1999. **109**(1): p. 70-8.

42. Fink, N., et al., *Mathematical analysis of atelectasis formation in middle ears with sealed ventilation tubes.* Acta Physiol Scand, 2003. **177**(4): p. 493-505.

43. Weibel, E.R., *The pathway for oxygen : structure and function in the mammalian respiratory system*. 1984, Cambridge, Mass.: Harvard University Press. xv, 425.

44. Weibel, E.R., et al., *Morphometric model for pulmonary diffusing capacity. I. Membrane diffusing capacity.* Respir Physiol, 1993. **93**(2): p. 125-49.

45. Weibel, E.R., *Stereological Methods. Practical Methods for Biological Morphometry.* Vol. 1. 1979, London: Academic.

46. Ars, B., et al., *Histomorphometric study of the normal middle ear mucosa. Preliminary results supporting the gas-exchange function in the postero-superior part of the middle ear cleft.* Acta Otolaryngol, 1997. **117**(5): p. 704-7.

47. Hunt, E.H. and D.R. Space, *The Airplane Cabin Environment.* 1994.

48. Harell, M., et al., *Gas composition of the human nose and nasopharyngeal space.* Acta Otolaryngol, 1996. **116**(1): p. 82-4.

49. Cantekin, E.I., W.J. Doyle, and C.D. Bluestone, *Comparison of normal eustachian tube function in the rhesus monkey and man.* Ann Otol Rhinol Laryngol, 1982. **91**(2 Pt 1): p. 179-84.

50. Cantekin, E.I., et al., *Airflow through the eustachian tube.* Ann Otol Rhinol Laryngol, 1979. **88**(5 Pt 1): p. 603-12.

51. Tideholm, B., B. Carlborg, and M. Brattmo, *Continuous long-term measurements of the middle ear pressure in subjects with symptoms of patulous eustachian tube.* Acta Otolaryngol, 1999. **119**(7): p. 809-15.

52. Koc, A., et al., *Evaluation of the mastoid air cell system by high resolution computed tomography: three-dimensional multiplanar volume rendering technique.* J Laryngol Otol, 2003. **117**(8): p. 595-8.

53. Cinamon, U. and J. Sade, *Mastoid and tympanic membrane as pressure buffers: a quantitative study in a middle ear cleft model.* Otol Neurotol, 2003. **24**(6): p. 839-42.

54. Cinamon, U. and J. Sade, *Tympanometry versus direct middle ear pressure measurement in an artificial model: is tympanometry an accurate method to measure middle ear pressure?* Otol Neurotol, 2003. **24**(6): p. 850-3.

55. Groth, P., et al., *Eustachian tube function in selection of airmen.* Aviat Space Environ Med, 1980. **51**(1): p. 11-7.

56. Alper, C.M., W.J. Doyle, and J.T. Seroky, *Higher rates of pressure decrease in inflamed compared with noninflamed middle ears.* Otolaryngol Head Neck Surg, 1999. **121**(1): p. 98-102.

57. Bylander, A., *Comparison of eustachian tube function in children and adults with normal ears.* Ann Otol Rhinol Laryngol Suppl, 1980. **89**(3 Pt 2): p. 20-4.

58. Bylander, A., *Function and dysfunction of the eustachian tube in children.* Acta Otorhinolaryngol Belg, 1984. **38**(3): p. 238-45.

59. Lildholdt, T., et al., *Effect of a topical nasal decongestant on Eustachian tube function in children with tympanostomy tubes.* Acta Otolaryngol, 1982. **94**(1-2): p. 93-7.

60. Cantekin, E.I., C.D. Bluestone, and L.P. Parkin, *Eustachian tube ventilatory function in children.* Ann Otol Rhinol Laryngol, 1976. **85**(2 Suppl 25 Pt 2): p. 171-7.

61. Federspiel, W.J. and A.S. Popel, *A theoretical analysis of the effect of the particulate nature of blood on oxygen release in capillaries.* Microvasc Res, 1986. **32**(2): p. 164-89.

62. Federspiel, W.J., *Pulmonary diffusing capacity: implications of two-phase blood flow in capillaries.* Respir Physiol, 1989. **77**(1): p. 119-34.

63. Yoon, T.H., et al., *Morphometric studies of the continuum of otitis media.* Ann Otol Rhinol Laryngol Suppl, 1990. 148: p. 23-7.

64. Hsia, C.C., C.J. Chuong, and R.L. Johnson, Jr., Red cell distortion and conceptual basis of diffusing capacity estimates: finite element analysis. J Appl Physiol, 1997. 83(4): p. 1397-404.

65. Frank, A.O., C.J. Chuong, and R.L. Johnson, A finite-element model of oxygen diffusion in the pulmonary capillaries. J Appl Physiol, 1997. 82(6): p. 2036-44.

66. Hsia, C.C., C.J. Chuong, and R.L. Johnson, Jr., Critique of conceptual basis of diffusing capacity estimates: a finite element analysis. J Appl Physiol, 1995. 79(3): p. 1039-47.

67. Hughes, J.M. and D.V. Bates, Historical review: the carbon monoxide diffusing capacity (DLCO) and its membrane (DM) and red cell (Theta.Vc) components. Respir Physiol Neurobiol, 2003. 138(2-3): p. 115-42.